

## CHAPTER VI

### Hydrogen bond spectroscopy in the near IR via combination bands: out-of-plane torsion and anti-gearred bending modes in (HF)<sub>2</sub>

#### 6.1 Introduction

As discussed in the previous chapter, the hydrogen fluoride dimer (HF)<sub>2</sub> has long served as a simple molecular paradigm for detailed study of hydrogen bonding properties. (HF)<sub>2</sub> is particularly attractive both from an experimental and theoretical point of view, due to the limited number of internal degrees of freedom ( $3N-6=6$ ) and small total electron count (20). An extensive succession of high-resolution spectroscopic studies of (HF)<sub>2</sub> in the microwave,<sup>1-4</sup> far-IR<sup>5-8</sup> and near-IR<sup>9-19</sup> spectral regions have led to accurate determination of vibrationally averaged structural parameters, interconversion tunneling rates, intramolecular vibrational frequencies, photofragment distributions and the hydrogen bond dissociation energy ( $D_0$ ). Considerably less is spectroscopically known about the intermolecular degrees of freedom, which are most directly sensitive to the angular-radial dependence (i.e., the global “shape”) of the hydrogen bond potential. The relatively limited information on these low frequency modes has made the most direct and rigorous comparisons between experiment and theory significantly more difficult. As one example specifically addressed in this

chapter, the spectroscopic information on these intermolecular modes is essential to include correctly zero-point contributions in any quantitative comparison of the equilibrium binding energy ( $D_e$ ), which comes directly from *ab initio* calculations, with the dissociation energy ( $D_0$ ) determined from experiment. It is worth noting that due to large amplitude motion of the light H atoms the difference between  $D_0$  and  $D_e$  proves to be quite significant, i.e., more than 50% of  $D_0$  itself.

There has been considerable theoretical effort<sup>20-42</sup> aimed at understanding the intermolecular forces in (HF)<sub>2</sub>, with a major goal being to model and interpret the high resolution dimer experimental data. High level *ab initio* techniques have been used to calculate both the binding energy and equilibrium structure of the dimer. From these calculations, frequency estimates of the four intermolecular modes have been obtained using the harmonic force fields determined from the curvatures of the potential energy at the minimum energy configuration. However, due to large amplitude, anharmonic motion in the hydrogen bonded vibrational modes, such harmonic predictions provide only relatively crude estimates of the true intermolecular vibrational frequencies. Alternatively, less sophisticated *ab initio* techniques have been used to calculate a sufficiently large number of potential energy points to permit an analytical multidimensional potential energy surface to be constructed. Two such potentials, which are analytical functions of all 6 internal degrees of freedom, are the *ab initio* surface of Bunker *et al.*,<sup>28,34</sup> (BJKLLK) and the semi-empirical surface of Quack and Suhm (SQSBDE).<sup>39</sup> Both surfaces are based on the same *ab initio* points of Kofranek

*et al.*<sup>30</sup> as a starting point, but the Quack and Suhm surface has been empirically adjusted to adequately reproduce available experimental quantities such as the dissociation energy and ground state  $\bar{B}$  rotational constant.

Though essential, the availability of a trial 6-D potential surface is only one step in the process; one also requires methods to solve accurately for the large amplitude quantum 6-D motion of the nuclei. This is an area which has been the focus of intense research effort;<sup>39,40,43-50</sup> recent developments in multidimensional quantum mechanics now allow solution of the corresponding full 6-D bound state eigenfunctions and eigenvalues for diatom-diatom systems such as HF dimer.<sup>46,48,49</sup> Thus, fully converged predictions for the four intermolecular vibrational modes now exist for both potentials listed above, which implicitly include all zero-point and anharmonic effects. This is particularly exciting, since such predictions of the intermolecular frequencies provide an essential link between experimental measurement and further refinement of the hydrogen bond potential surface. In addition, since the intermolecular vibrations sample portions of the multidimensional potential energy surface significantly different from the ground state, direct observation of these intermolecular modes offers a rigorous and independent test of the accuracy of such surfaces. As we shall see, even though quite reasonable agreement exists between theory and experiment for the dissociation energy ( $D_0$ ) and equilibrium configuration of  $(\text{HF})_2$ , considerable uncertainties still remain in the global accuracy of these potentials, especially sampling at intermolecular vibrational geometries far from

the equilibrium configuration.

The four zero-order intermolecular vibrational modes in (HF)<sub>2</sub> correspond to angular/radial motion predominantly in the “van der Waals stretch” ( $\nu_4$ ), in-plane “geared” ( $\nu_5$ ) and “anti-geared” ( $\nu_3$ ) bends, and out-of-plane torsion ( $\nu_6$ ) of the two HF subunits. From previous experimental efforts in both the near<sup>15,16</sup> and far-IR,<sup>5-8,51</sup> the two lower intermolecular modes, the “van der Waals stretch” ( $\nu_4$ ) and “geared bend” ( $\nu_5$ ) are known to be at 125.1 and 160.6 cm<sup>-1</sup>, respectively, while the out-of-plane torsion ( $\nu_6$ ,  $K = 1$ ) is significantly higher at 399.78 cm<sup>-1</sup>. Prior to this study, the fourth and highest energy intermolecular mode,  $\nu_3$ , had not been observed but is predicted from 6-D quantum calculations<sup>5-8,46,51</sup> to be around 425 cm<sup>-1</sup>. Classically, this  $\nu_3$  vibration corresponds to an “anti-geared” bend motion, i.e., frustrated internal rotation of the two HF monomers in the *same* direction. The relatively high frequency of this in-plane bending mode arises because motion along this coordinate quickly breaks the donor-acceptor hydrogen bond. For in-plane configurations of HF dimer, there also exists a much lower energy angular channel along the so-called “geared” bend coordinate, where the two HF monomers counter rotate in *opposite* directions. This lower energy path is largely responsible for the interconversion tunneling motion in (HF)<sub>2</sub>, and results in the well-known splitting of the rovibrational levels evidenced in all (HF)<sub>2</sub> spectra. Thus, the anti-geared and geared bend vibrations map out the *in-plane* portions of the potential surface responsible for tunneling phenomena. The corresponding torsional degree of freedom on the potential surface is

predominantly sampled by the *out-of-plane*  $\nu_6$  torsional vibration, which corresponds to an azimuthal twisting of the subunits around the intermolecular axis defined by the two HF centers of mass axis.

One must be cautious when trying to assign descriptive quantum labels to these intermolecular vibrations. Specifically, for relatively weak restoring forces and highly anharmonic potentials, there can be considerable mixing between the different degrees of freedom that render such descriptive labels approximate. As one especially relevant case in point, the two nearly degenerate  $\nu_4$  and  $\nu_5$  modes, which correspond nominally to van der Waals stretch and geared bend excitation, have been shown in the last chapter to be substantially mixed in (HF)<sub>2</sub>. However, due to a combination of vibrational symmetry and energy separation, this is less likely to be the case among the two higher frequency  $\nu_3$  and  $\nu_6$  intermolecular modes. For example, the  $\nu_6$  mode is the lowest energy out-of-plane ( $\Gamma_{\text{vib}} = A^-$ ) mode, and therefore rigorously can not couple with any overtone or combination state of the in-plane vibrations ( $\Gamma_{\text{vib}} = A^+/B^+$ ). Conversely, though the anti-geared bend mode is not prevented by symmetry from mixing with the other two in-plane intermolecular vibrational states, its relatively high vibrational frequency keeps it “detuned” from fundamentals and low order combination bands of the other even parity states.

Previous combination band studies in our laboratory of the intermolecular modes built on one quantum of high frequency intramolecular excitation have demonstrated the unique advantages of the near-IR method (see Chapter V).

Specifically, the use of near-IR laser light sources offers *continuous*, single mode tuning over spectral regions as large as several thousand  $\text{cm}^{-1}$ . This makes possible extensive high resolution searches for  $(\text{HF})_2$  combination spectra, and reliably establishes the relative integrated intensities of these bands. As an important corollary, this capability also allows us to indicate when bands are *not observed*, and therefore to quantify lower limits on the experimental band strengths. In addition, the use of a slit supersonic expansion source permits large concentrations of dimer species at low vibration/translation/rotational temperatures (10K), and with long direct absorption path lengths ideally suited for spectroscopic detection at high sensitivity. This combination of long path length, high cluster concentration, and near shot noise limited absorbance permits detection of combination bands as much as 1000-fold weaker than the strongest intramolecular fundamentals, which has made possible observation of all *four*  $(\text{HF})_2$  intermolecular modes in the near-IR. Finally, since the near-IR excitation frequency exceeds the dissociation energy of the complex, vibrational predissociation in the upper state can and does occur. This opens a new dynamical channel not accessible in the far-IR, the rates of which can be obtained from high resolution measurements of the homogeneous broadening for individual rovibrational transitions.

In the present study, both the “high” energy intermolecular modes  $\nu_3$  and  $\nu_6$  are observed in combination with either the  $\nu_1$  or  $\nu_2$  HF-stretch intramolecular vibrations. In conjunction with the well-established intramolecular fundamental

data,<sup>5,9,10,13</sup> this permits accurate measurement of both the intermolecular frequencies and tunneling splittings in the HF-stretch excited state manifold. Furthermore, linewidth measurements permit the dependence of HF-stretch induced vibrational predissociation lifetimes on intermolecular excitation to be elucidated. The linewidths measured for these combination states predominantly reflect a dependence on intramolecular mode, but also show a dependence on the intermolecular vibration consistent with trends first identified for the lower energy “van der Waals stretch” and “geared bend” combination bands. Reliable extrapolation to the corresponding  $\nu_3$  and  $\nu_6$  intermolecular fundamentals is possible based on the current near-IR measurements of the  $\nu_3$  and  $\nu_6$  combination bands. The predicted frequencies for  $\nu_6$  are in reasonable agreement, but the  $\nu_3$  value is considerably *underestimated* by the 6-D quantum calculations, indicating that further refinement of the current (HF)<sub>2</sub> potentials is necessary. This discrepancy also has important implications for the zero-point contributions to the dissociation energy due to the intermolecular modes, which are necessary to obtain experimental estimates of the ( $D_e$ ) binding energy.

### 6.3 Experiment

The experimental technique employed in this project is identical to that used in previous<sup>16</sup> studies of (HF)<sub>2</sub> and is described briefly in the previous chapter

and in detail in Chapter II. Specific to the current study, absolute frequency calibration of the  $\nu_2+\nu_6$  combination band ( $\sim 4290\text{ cm}^{-1}$ ) is made with respect to the R(0) transition ( $4263.837198\text{ cm}^{-1}$ ) of the first overtone of CO.<sup>52</sup> Similarly, the  $\nu_1+\nu_3$  combination band ( $\sim 4418\text{ cm}^{-1}$ ) is referenced to the R(3) transition ( $4420.6480(2)\text{ cm}^{-1}$ ) of the first overtone of the anti-symmetric stretch of N<sub>2</sub>O.<sup>53</sup> This calibration procedure allows the transition frequencies and vibrational origins to be reported to an absolute accuracy of  $0.0004\text{ cm}^{-1}$ .

### 6.3 Results and analysis

Based on previous far-IR experimental data<sup>5</sup> and predictions of the intermolecular mode frequencies,<sup>46</sup> the search for HF dimer combination bands associated with the two “high” frequency intermolecular modes ( $\nu_3$  and  $\nu_6$ ) covers the  $200\text{ cm}^{-1}$  region between  $4280$  and  $4480\text{ cm}^{-1}$ . An exhaustive search over this region reveals only 4 VRT bands; these bands reflect excitation in each of the  $\nu_3$  and  $\nu_6$  intermolecular modes, built on either the  $\nu_1$  or  $\nu_2$  intramolecular fundamentals. A stick spectrum that schematically summarizes the vibrational origins and relative integrated intensities for the combination bands reported in this chapter is shown in Figure 6.1, along with similar data on the “low” frequency  $\nu_4$  and  $\nu_5$  combination bands observed previously and discussed in the previous chapter. Note that the  $\nu_2+\nu_6$  combination band is relatively strong, i.e.,

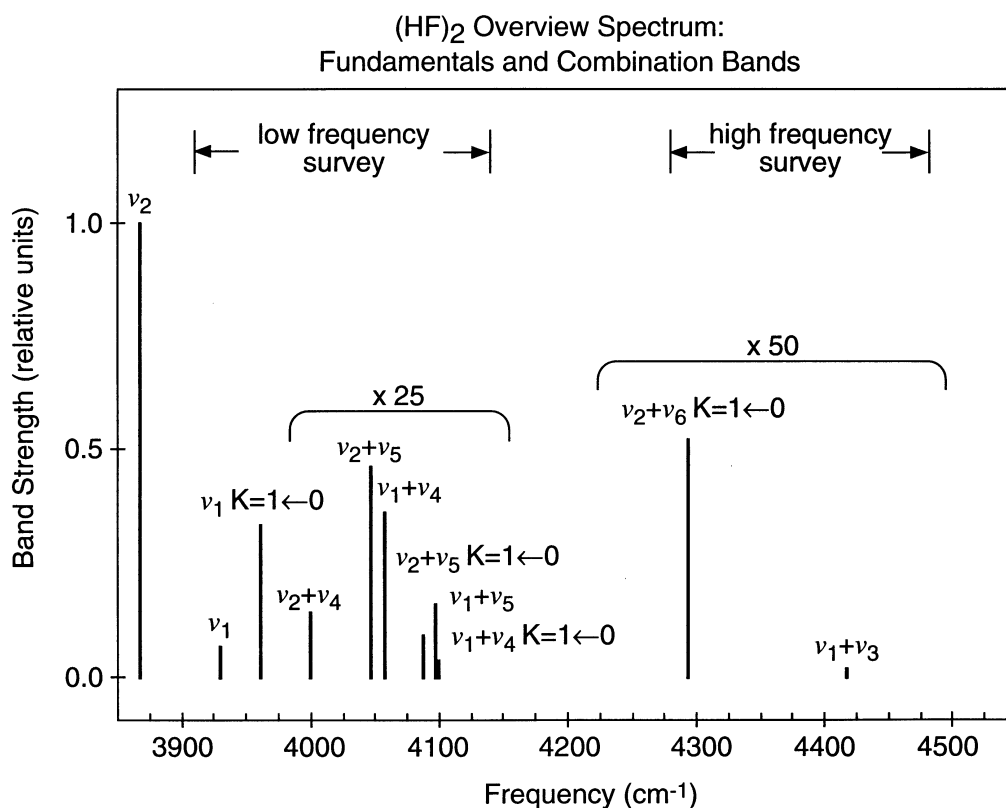


Figure 6.1 Overview of the near-IR fundamental and combination band spectrum of (HF)<sub>2</sub> in a slit jet. Indicated in the spectrum are the two spectral regions surveyed for combination bands. A “low” frequency region from 3850-4200 cm<sup>-1</sup> and a “high” frequency region from 4280-4480 cm<sup>-1</sup>. The results of the “low” frequency search have been reported elsewhere, while this paper focuses on the “high” frequency results. The transition strengths of the combination bands have been multiplied by 25 and 50 in order to plot the combination bands on the same scale as the intramolecular fundamentals. Only one of the tunneling components are shown for each fundamental and combination band.

down by only 95-fold from the  $\nu_2$   $K = 0 \leftarrow 0$  fundamental band ( $K = K_a$ ).

However, the  $\nu_1 + \nu_3$  combination band is the weakest observed in  $(\text{HF})_2$ , down in intensity by nearly a factor of 2500 from the  $\nu_2$  fundamental.

### 6.3.1 Out-of-plane torsion ( $\nu_6$ )

#### $(\nu_2 + \nu_6) K = 1 \leftarrow 0$

Based on the low rotational temperatures achieved in the slit jet expansion and the symmetry requirements<sup>54-58</sup> for dipole mediated transitions in  $(\text{HF})_2$ , perpendicular  $K = 1 \leftarrow 0$  transitions are anticipated to be strongest for combination bands with one quantum of  $\nu_6$  excitation. The two possible near-IR frequencies for these  $K = 1 \leftarrow 0$  bands can be crudely estimated by adding the frequency of the ( $K = 1 \leftarrow 0$ ) out-of-plane torsion fundamental measured in the far-IR<sup>5</sup> to either the  $\nu_1$  or  $\nu_2$  fundamental frequency.<sup>10</sup> Furthermore, due to stronger hydrogen bonding in the intramolecular frequencies, the combination bands should be somewhat blueshifted from these predictions. Qualitatively consistent with these expectations, a strong  $K = 1 \leftarrow 0$  subband of  $(\text{HF})_2$  is observed at  $4293 \text{ cm}^{-1}$  (approximately 100-fold weaker than the  $\nu_2$   $K = 0 \leftarrow 0$  fundamental), which is close to but at a higher energy than the  $400 \text{ cm}^{-1} + 3868 \text{ cm}^{-1} = 4268 \text{ cm}^{-1}$  origin one estimates for the  $\nu_2 + \nu_6$  band. Conversely, the  $\nu_1 + \nu_6$  band would be predicted at  $4331 \text{ cm}^{-1}$ , which is already higher than observed experimentally. Shown in Figure 6.2 is a section of the spectrum containing the  $Q$ -branch region for the two VRT bands, one for each tunneling level. Lower state combination differences

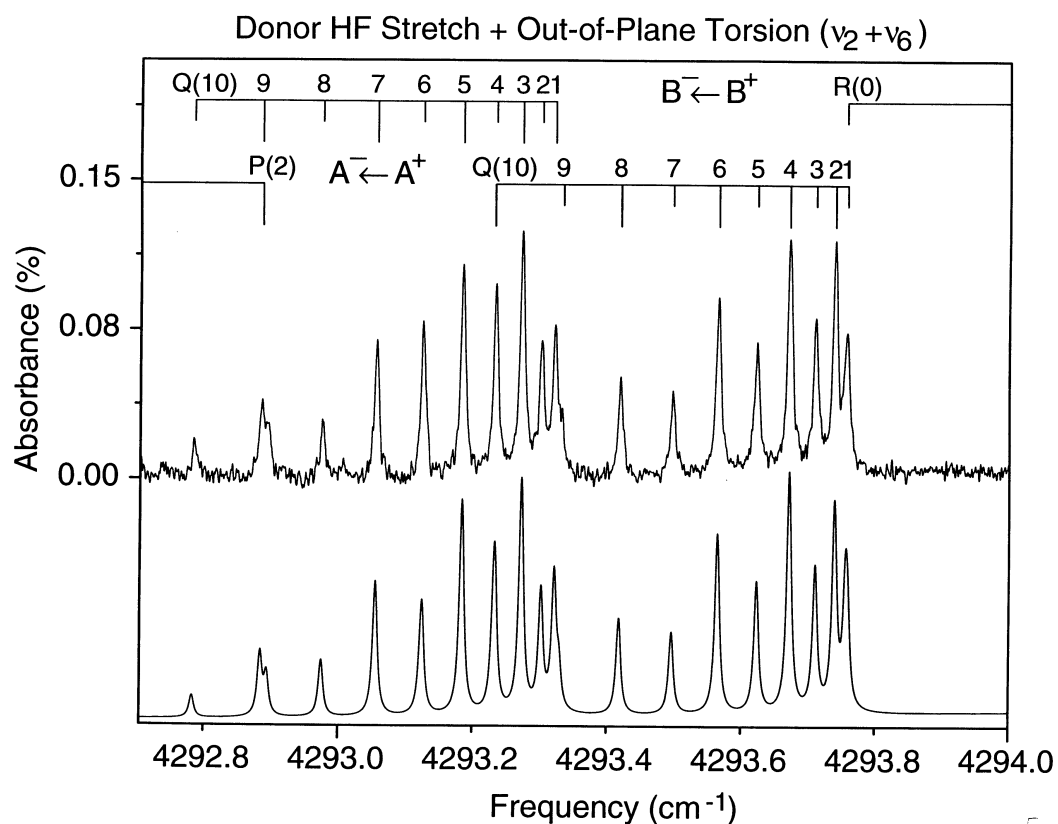


Figure 6.2 A section of the spectrum near the origin of the  $K = 1 \leftarrow 0$  subband of the  $\nu_2 + \nu_6$  combination band of  $(\text{HF})_2$ . The Q-branch is split into two rotational progression by the tunneling motion present in  $(\text{HF})_2$ . The  $A^+$  and  $B^+$  symmetry labels refer to  $\Gamma_{\text{vib-tun}}$ , the vibration-tunneling symmetry. The simulated spectrum at the bottom of the figure was calculated using the rotational constants determined from the spectroscopic fit, and the rotational temperature  $T_{\text{rot}} = 10(1)$  K and predissociation broadening (250(20) MHz) were determined from a least squares fit to the data (see text for details).

calculated using the corresponding *R*- and *P*-branch transitions ( $\sigma_{\text{rms}}=0.0005 \text{ cm}^{-1}$ ) indicate unambiguously that these transitions arise from the  $K = 0$  state of HF dimer.

In addition, these combination differences can be used to assign the ground state tunneling symmetry for each VRT band, which are further verified by the intensity alternation apparent in Figure 6.2. Specifically, due to nuclear spin statistics, the intensity in even:odd  $J''$  is 10:6(6:10) for transitions originating from the  $\Gamma_{\text{vib-tun}} = A^+(B^+)$  level of the  $K = 0$  ground state, respectively. Symmetry assignments refer to the irreducible representations in the  $M_{S4}$  molecular symmetry group and are discussed in more detail in the previous chapter. All transitions from *R*(9) through *P*(5), including *Q*(1)-*Q*(9), are observed for each VRT band and reported in Table 6.1. The rotational progressions for each VRT band are fit separately to Eq. (6.1);

$$E_K(J) = \nu_K + [\bar{B}_K \pm 1/4 b_K \delta_{K1}]J(J + 1) - D_K J^2(J + 1)^2 + H_K J^3 (J + 1)^3 \quad (6.1)$$

In Eq. (6.1)  $\nu_K$  is defined to be the energy of the  $J = 0$  (extrapolated for  $K > 0$ ) state for a given  $K$  level. In addition,  $\bar{B}_K$ ,  $D_K$  and  $H_K$  are the  $K$ -dependent effective rotational and distortion constants in symmetric top notation, while the Kronecker delta  $\delta_{K1}$  brings in an asymmetry splitting term due to  $b_K = (B_K - C_K)$

Table 6.1 Transition frequencies (in  $\text{cm}^{-1}$ ) for the  $\nu_2+\nu_6$   $K=1\leftarrow 0$  and  $\nu_1+\nu_3$   $K=0\leftarrow 0$  VRT bands in  $(\text{HF})_2$ . The  $A^\pm/B^\pm$  symmetry labels refer to  $\Gamma_{\text{vib-tun}}$ .

	$\nu_2+\nu_6$ $K=1\leftarrow 0$		$\nu_1+\nu_3$ $K=0\leftarrow 0$	
	$A^- \leftarrow A^+$	$B^- \leftarrow B^+$	$B^+ \leftarrow A^+$	$A^+ \leftarrow B^+$
R(8)	4297.2669(-3)		4421.1431(-1)	4420.6078(-1)
R(7)	4296.9158(3)	4296.4647(0)	4420.8459(4)	4420.3137(2)
R(6)	4296.5546(3)	4296.1058(-6)	4420.5328(3)	4420.0042(3)
R(5)	4296.1834(-3)	4295.7386(3)	4420.2042(-1)	4419.6792(4)
R(4)	4295.8036(-2)	4295.3604(0)	---- <sup>f</sup>	4419.3388(4)
R(3)	4295.4143(-4)	4418.9733(4)	4419.5022(-2)	4418.9828(3)
R(2)	4295.0163(-3)	4294.5764(4)	4419.1291(2)	4418.6114(3)
R(1)	4294.6091(-5)	4294.1699(-1)	4418.7404(0)	4418.2246(3)
R(0)	4494.1936(0)	---- <sup>a</sup>	4418.3371(3)	4417.8219(-1)
Q(1)	4293.7574(-19) <sup>b</sup>	4293.3206(-2)		
Q(2)	4293.7397(-2)	4293.3011(-2)		
Q(3)	4293.7105(-4)	4293.2717(-2)		
Q(4)	4293.6715(-6)	4293.2324(-2)		
Q(5)	4293.6231(-4)	4293.1832(-1)		
Q(6)	4293.5655(4)	4293.1236(-2)		
Q(7)	4293.4974(7)	4293.0543(2)		
Q(8)	4293.4180(-3)	4292.9739(-1)		
Q(9)	---- <sup>c</sup>	4292.8842(10) <sup>d</sup>		
Q(10)		4292.7818(1)		
P(1)			4417.4844(-5)	4416.9714(3)
P(2)	4292.8941(6)	4292.4573(18) <sup>e</sup>	4417.0369(3)	4416.5222(-4)
P(3)	4292.4438(11)	4292.0043(-2)	4416.5739(3)	4416.0589(1)
P(4)	4291.9834(0)	4291.5451(4)	4416.0950 (1)	4415.5796(-2)
P(5)	4291.5163(8)	4291.0763(2)	4415.6032(0)	4415.0853(-4)
P(6)	4291.0388(-1)		4415.0961(1)	4414.5759(-6)
P(7)			4414.5759(16) <sup>g</sup>	4414.0522(-2)
P(8)			4414.0380(-1)	4413.5130(-6)
P(9)			4413.4872(-3)	

a. overlap with Q(1) of  $A^- \leftarrow A^+$

b. overlap with R(0) of  $B^- \leftarrow B^+$

c. overlap with Q(1) of  $B^- \leftarrow B^+$

d. overlap with P(2) of  $A^- \leftarrow A^+$

e. overlap with Q(9) of  $B^- \leftarrow B^+$

f. overlap with R(3) of  $\text{N}_2\text{O}$

g. overlap with P(3) of  $\text{N}_2\text{O}$

which is only significant for  $K = 1$  levels. For the spectra presented in this chapter, the ground state constants are held fixed at values determined from global fits to both microwave and near-IR data, which have been presented elsewhere.<sup>8,17,38</sup> Furthermore, upper state sextic centrifugal distortion constants,  $H_K$ , are set to zero due to the lack of high  $J$  transitions necessary for an accurate determination. The results of the fits to Eq.(6.1) are summarized in Table 6.2. A comparison of the experimental data with a simulated spectrum generated using a sum of Voigt lineshapes and the constants reported in Table 6.2 is also shown in Figure 6.2. Excellent agreement between experiment and the simulated spectrum, both in frequency and relative intensities, is achieved for a slit jet temperature of 10(1)K and a  $J$  independent vibrational predissociation broadening of 250(20) MHz.

The  $\nu_2$  *intramolecular* assignment of this band to  $\nu_2$  is first suggested by the much better agreement between predicted and observed vibrational origins for  $\nu_2+\nu_6$  vs.  $\nu_1+\nu_6$  excitation, but is also confirmed by a combination of linewidth and tunneling symmetry arguments. From a high resolution linewidth analysis discussed in section 6.5, the transition profiles are dominated by 250(20) MHz contributions from predissociation broadening. This is comparable to the 330 MHz predissociation linewidth measured<sup>13</sup> for  $\nu_2$  and yet > 20-fold larger than the 10 MHz values observed in  $\nu_1$ . This strongly indicates a combination band built on  $\nu_2$  based on the relatively weak dependence of vibrational predissociation on intermolecular mode observed in our previous studies of  $\nu_4$  and  $\nu_5$ . Additional

Table 6.2 Molecular constants ( $\text{cm}^{-1}$ ) from spectral fits of the combination bands assigned to the ( $\nu_6$ ) out-of-plane torsion and ( $\nu_3$ ) anti-g geared bend. All origins are reported with respect to the  $\Gamma=A^+$   $K=0$  ground vibrational state of  $(\text{HF})_2$ . The uncertainties in parentheses represent  $2\sigma$  in the units of the last reported digit.

$\Gamma_{\text{vib-tun}} =$	$\nu_2 + \nu_6, K = 1$		$\nu_1 + \nu_3, K = 0$	
	$A^-$	$B^-$	$B^+$	$A^+$
$\nu_0$	4293.7690(5)	4293.9893(3)	4417.9183(3)	4418.0629(3)
$\bar{B}$	0.212117(32)	0.211900(16)	0.20926(2)	0.20887(2)
$D_K/10^{-6}$	2.58(40)	3.03(16)	1.96(26)	1.48(26)
$b_K/10^{-3}$	0.949(26)	0.825(15)	----	----
$\sigma_{\text{rms}}$	0.00053	0.00030	0.00034	0.00037

corroboration of the  $\nu_2$  intramolecular assignment is obtained from the energy ordering of the tunneling levels in the upper vibrational state. Based on an intermolecular assignment to the out-of-plane torsion, the origins of the two VRT bands are consistent with  $\Gamma_{\text{vib}} = \Gamma_{\text{intra}} \otimes \Gamma_{\text{inter}} = A^-$ , and thus a  $\nu_2$  ( $\Gamma_{\text{intra}} = A^+$ ) intramolecular mode assignment. Specifically, this assignment implies an  $A^+/B^+$  ordering of tunneling symmetry levels in the  $\nu_2+\nu_6$  state and thus a positive tunneling splitting. Indeed, in all 14 VRT bands observed in combination with the  $\nu_1/\nu_2$  dyad in HF dimer, we have found no exception to this pattern, i.e., all vibrational assignments indicate the  $\Gamma_{\text{tun}} = A^+$  tunneling level to be the lower energy state in each tunneling pair.

As a test of internal consistency, the sign of the asymmetry splitting leads to the identification of these VRT bands as *C*-type, and thus that the vibrational

parity of the upper state is commensurate with the out-of-plane torsion  $\nu_6$  *intermolecular* vibrational assignment. The resulting intermolecular vibrational energy is obtained by subtracting the  $\nu_2$  fundamental ( $3868.0793(2) \text{ cm}^{-1}$ ) from the energy of the (lower)  $\Gamma_{\text{tun}} = A^+$  state, yielding an intermolecular energy of  $425.6897(5) \text{ cm}^{-1}$  for the  $K = 1$  state of the out-of-plane torsion. As anticipated, there is an appreciable increase (+6.5%) in the  $\nu_6$  intermolecular frequency measured in the  $\nu_2$  excited state relative to the far-IR  $\nu_6$  measurement ( $399.787(1) \text{ cm}^{-1}$ ), consistent with a “stiffening” of the hydrogen bond in the HF-stretch excited states. In order to isolate the effect of  $\nu_6$  excitation on vibrationally averaged geometries in both the ground and  $\nu_2$  excited states, the changes in rotational  $\bar{B}$  and  $D$  constants are calculated with respect to the corresponding state without  $\nu_6$  excitation. The changes in these constants upon  $\nu_6$  excitation are remarkably similar in the far- and near-IR. In both cases the  $\bar{B}$  rotational constant decreases by approximately 3%, corresponding roughly to a 1.5% increase in the hydrogen bond length ( $\bar{B} \propto \langle 1/R^2 \rangle$ ). Consistent with this elongation of the hydrogen bond, the  $D$  distortion constants increase in the  $\nu_6$  excited state, indicating a reduced hydrogen bond restoring force. One simple physical interpretation of this rotational analysis is that *non-planar* configurations lead systematically to a *weaker*, and therefore *longer*, hydrogen bond. This also provides corroborating evidence for relatively weak coupling between inter and intramolecular degrees of freedom, i.e., while  $\nu_2$  excitation increases the  $\nu_6$  intermolecular energy, it does not dramatically influence the intermolecular character of the  $\nu_6$  vibration.

For  $\nu_2+\nu_6$  excitation ( $\Gamma_{\text{vib}} = A^-$ ), the *difference* in the two VRT band origins equals the *increase* in the tunneling splitting between the lower and upper vibrational state. The tunneling splitting in the upper state is therefore determined to be  $0.2203(6) \text{ cm}^{-1}$ , which is 50% smaller than the tunneling splitting in the  $\nu_2$   $K = 1$  state ( $\Delta v_{\text{tun}} = 0.3411(9) \text{ cm}^{-1}$ ). This relatively small change in the tunneling splitting in the  $\nu_6$  intermolecular excited state is somewhat consistent with far-IR measurements, where the tunneling splitting increases only slightly from  $1.0644374(1) \text{ cm}^{-1}$  in the  $K = 1$  ground state to  $1.626(1) \text{ cm}^{-1}$  in the  $\nu_6$   $K = 1$  excited state. Thus, unlike the dramatic 5-10 fold increases in tunneling splitting measured for both  $\nu_4$  and  $\nu_5$  excitation, this “high” energy intermolecular mode appears to have only a relatively modest ( $\approx 50\%$ ) effect on the interconversion tunneling splitting. We return to a more detailed analysis of the intermolecular mode specific tunneling dynamics in the discussion section.

As one final point, the analogous combination band built on the “free” HF-stretch ( $K = 1 \leftarrow 0$  band of  $\nu_1+\nu_6$ ) is *not* experimentally observed. Given the transition strength and S/N of the  $\nu_2+\nu_6$   $K = 1 \leftarrow 0$  combination band, the corresponding band built on  $\nu_1$  should be easily detectable. Furthermore, the anticipated blue shift of  $\nu_1+\nu_6$  from the  $\nu_2+\nu_6$  origin can be readily estimated from the differential  $\nu_1/\nu_2$  fundamental shifts to within a few  $\text{cm}^{-1}$  uncertainty; thus spectral search is not an issue. From previous work with the lower energy  $\nu_4$  and  $\nu_5$  (HF)<sub>2</sub> combination bands, the  $\nu_1+\nu_6$  combination band transitions would be anticipated to be as much as an order of magnitude *narrower* than in the  $\nu_2+\nu_6$

combination band; this should make detection using high resolution spectroscopy even easier since the same integrated band strength is collapsed into sharper lines. Despite these experimental advantages, however, we have not been able to observe the  $K = 1 \leftarrow 0$  combination band. Based on the S/N and linewidth considerations the  $\nu_1 + \nu_6$  band must be down at least a factor of 200 in transition strength from the corresponding  $\nu_2 + \nu_6$  band. This is one of several examples of anomalous intensity effects seen in both the HF and DF dimer combination band spectra, which are *not even qualitatively* explained by full 6-D calculations on trial potential surfaces.

### 6.3.2 Anti-gearred bend ( $\nu_3$ )

#### $(\nu_1 + \nu_3) K = 0 \rightarrow 0$

Prior to the present study, the anti-gearred bend ( $\nu_3$ ) in  $(\text{HF})_2$  had not been observed either in the far-IR or via combination bands in the near-IR, though full 6-D quantum calculations<sup>13,46</sup> on the best available potential surfaces predicted it to be around  $425 \text{ cm}^{-1}$ . Initial search efforts to observe  $\nu_1 + \nu_3$  were guided by these numbers, centered around  $3931 \text{ cm}^{-1} + 425 \text{ cm}^{-1} = 4360 \text{ cm}^{-1}$ . Despite an exhaustive single mode search, no bands due to HF dimer are evident in a  $50 \text{ cm}^{-1}$  window around this region. However, approximately  $60 \text{ cm}^{-1}$  *further to the blue* of the original estimate, two weak overlapping bands ( $\sim 0.1\%$  the integrated

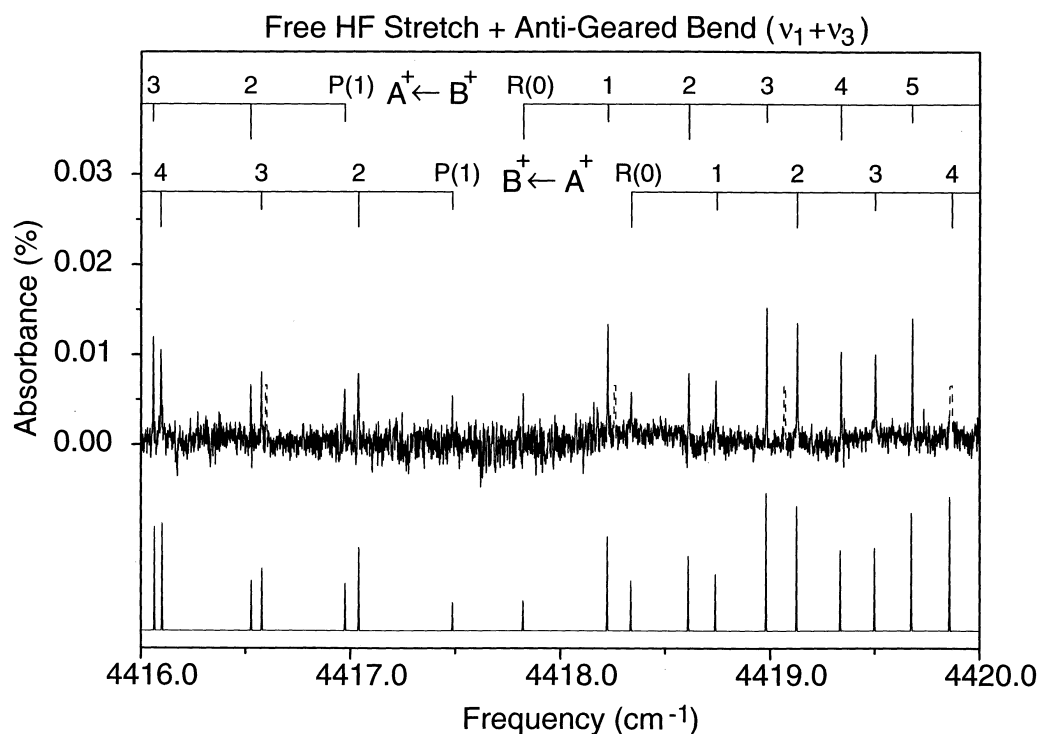


Figure 6.3 Spectral region near the origins of the two  $K = 0 \leftarrow 0$  VRT bands of the  $\nu_1 + \nu_3$  combination band of  $(\text{HF})_2$ . The two VRT bands are nearly overlapping due to the small tunneling in the upper state and since the difference in the origins of the two bands reflects the difference between the tunneling splitting in the upper and lower vibrational states. The simulated spectrum was calculated using the rotational constants from the fit and a 10 K rotational temperature. Additional strong peaks are due to the  $(20^0) \leftarrow (00^0)$  rovibrational transitions of monomeric  $\text{N}_2\text{O}$  added to increase the  $(\text{HF})_2$  signal (see text) are also evident.

intensity of the  $K = 0 \leftarrow 0$   $\nu_1$  fundamental) are observed around  $4418 \text{ cm}^{-1}$ ; a section of the spectrum is shown in Figure 6.3. The simple  $P/R$ -branch structure for each VRT band, the presence of  $R(0)$  and  $P(1)$ , and the approximately  $4\bar{B} \approx 0.8 \text{ cm}^{-1}$  “null gap” confirm that each VRT band is a  $K = 0 \leftarrow 0$  band of  $(\text{HF})_2$ . Ground state combination differences ( $\sigma_{\text{rms}} = 0.0004 \text{ cm}^{-1}$ ) allow for unambiguous  $J''$  labeling of the transitions, as well as the  $\Gamma_{\text{vib-tun}}$  symmetry in the lower state. The symmetry assignments determined from combination differences are verified by intensity alternation in  $J$  present in the spectrum (see Figure 6.3). All transitions from  $R(8)$  to  $P(8)$ , inclusive, are observed for each of the two VRT bands and are reported in Table 6.1. The molecular constants obtained by fitting the rotational progressions for both VRT bands to Eq. (6.1) are summarized in Table 6.2. Included in Figure 6.3 is the simulated spectrum using the molecular constants determined from the fit and the 10 K slit jet temperature.

The relatively narrow predissociation linewidths measured for the individual rovibrational transitions (90(20) MHz and 60(20) MHz for the  $A^+ \leftarrow B^+$  and  $B^+ \leftarrow A^+$  VRT bands, respectively) suggest a  $\nu_1$  intramolecular assignment, though these are substantially broadened beyond the values for the pure  $\nu_1$  fundamental. This  $\nu_1$  assignment is additionally confirmed by the relative origins of the two VRT bands and the expectation of positive tunneling in the upper state. Specifically, the  $\Gamma_{\text{vib-tun}} = A^+ \leftarrow B^+$  origin is at higher frequency than the  $\Gamma_{\text{vib-tun}} = B^+ \leftarrow A^+$  origin, which means a  $\Gamma_{\text{vib-tun}} = B^+(A^+)$  symmetry for the lower (upper) tunneling level in the upper vibrational state. Thus, for the lower energy tunneling

level to have  $\Gamma_{\text{tun}} = A^+$  symmetry requires  $\Gamma_{\text{vib}} = \Gamma_{\text{intra}} \otimes \Gamma_{\text{inter}} = B^+$ , which for any in-plane intermolecular mode ( $\Gamma_{\text{inter}} = A^+$ ) implies the corresponding intramolecular vibration must be  $\nu_1$  ( $\Gamma_{\text{intra}} = B^+$ ). The intermolecular frequency is determined by subtracting the  $\nu_1$  fundamental ( $3930.9030(2) \text{ cm}^{-1}$ ) from the origin of the  $B^+ \leftarrow A^+$  VRT band, which yields  $487.0153(4) \text{ cm}^{-1}$ .

As this  $487 \text{ cm}^{-1}$  intermolecular mode is now almost one half the dissociation energy of HF dimer, the assignment of this intermolecular component to the  $\nu_3$  anti-gear bend requires more subtle consideration. Unlike the out-of-plane torsion, symmetry arguments alone are not sufficient; any of the three in-plane intermolecular vibrations (all  $\Gamma_{\text{inter}} = A^+$ ) or combinations thereof could conceivably give rise to this combination band. Thus, even though  $\nu_3$  is the only *fundamental* vibration of the correct  $\Gamma_{\text{inter}} = A^+$  symmetry predicted within  $300 \text{ cm}^{-1}$ , *multiply* excited  $\nu_4$  and  $\nu_5$  states are in principle accessible at this high an intermolecular energy.

Our assignment of this band to  $\nu_1 + \nu_3$  excitation is based on the following experimental data. First of all, any assignment not involving  $\nu_3$  would require at least *three* quanta of intermolecular excitation distributed between the low-frequency  $\nu_4$  and  $\nu_5$  intermolecular modes. Given the 25-fold reduction in the integrated intensity between the *strongest* binary combination band and intramolecular fundamental, one would anticipate such exotic combination bands with four quanta of inter/intramolecular excitation to be several orders of magnitude weaker than observed. Indeed, quantum calculations of far-IR

transitions strengths<sup>59</sup> support such a rapid drop off in intensity for the intermolecular overtones and combination bands. Secondly, both the  $\nu_4$  and  $\nu_5$  intermolecular modes have been found experimentally to increase the tunneling splitting in both the  $\nu_1$  and  $\nu_2$  excited states by 8-15 fold; thus any assignment that included *multiple* quanta in these two modes would be expected to exhibit an anomalous *large* tunneling splitting. By way of contrast, the tunneling splitting in the upper state is  $0.1447(4) \text{ cm}^{-1}$ , which is quite comparable and even a bit *smaller* than the corresponding  $0.2155(3) \text{ cm}^{-1}$  splitting in  $\nu_1$ . Third, continuous single mode spectral scans  $80 \text{ cm}^{-1}$  both to the red and blue of this band confirm this as the *only* state with sufficient oscillator strength for us to detect with the slit jet spectrometer. This  $160 \text{ cm}^{-1}$  region is certainly a sufficiently broad window to include the  $\nu_1+\nu_3$  combination band. Thus even though other (e.g.,  $\nu_1+3\nu_5$ ,  $\nu_1+3\nu_4$ ,  $\nu_1+\nu_4+2\nu_5$ ,  $\nu_2+3\nu_5$ , etc.) combination bands are also predicted to be in the region surveyed, it seems a highly unlikely scenario that  $\nu_1+\nu_3$  would *not* be observable while one (and only one) of these higher order combination bands would be detected. As a final confirmation and consistency test, analogous single mode spectral scans for all four intermolecular modes in DF dimer (presented in Chapter VIII) have also revealed only one “bright” state at intermolecular energies higher than the out-of-plane torsion, which we have assigned as the corresponding  $\nu_1+\nu_3$  combination band in  $(\text{DF})_2$ .

As discussed in the previous chapter, pure descriptive labels for these intermolecular states can be difficult to make unambiguously. Since  $\nu_3$  has  $\Gamma_{\text{inter}}=$

$A^+$  vibrational symmetry, it can in principle be mixed with any overtone/combination states of both van der Waals stretch and geared bend character. Indeed, the 4% decrease in the  $\bar{B}$  rotational constant between  $\nu_1+\nu_3$  and  $\nu_1$  may already indicate partial van der Waals stretch character in the  $\nu_3$  intermolecular state due to radial-angular coupling for motion along the anti-geared bending coordinate. Such an interpretation is qualitatively corroborated by analysis of eigenfunction nodal patterns from full 6-D quantum calculations.<sup>46</sup> However, since this is the only “bright” combination state experimentally observed within  $\pm 80 \text{ cm}^{-1}$  of the  $(\text{HF})_2$  frequency region anticipated for  $\nu_3$ , this intermolecular state has at least significant if not predominantly anti-geared bend character. A more descriptive intermolecular mode assignment will be discussed in the comparison with theory.

## 6.4 Discussion

### 6.4.1 Donor-acceptor interchange tunneling

In a molecule such as  $(\text{HF})_2$  that has four intermolecular degrees of freedom and only one low energy tunneling coordinate (corresponding approximately to a “geared” rotation of the HF subunits), intermolecular excitation might be expected to increase the donor-acceptor tunneling rate in a strongly mode specific fashion. Due to spectral congestion in cooled cell far-IR

studies,<sup>5-8</sup> however, there has been little data available for the tunneling splittings in intermolecular excited states with which to test such predictions. For example, the only previous far-IR direct experimental observation<sup>5</sup> of a tunneling splitting for an intermolecular excited state is for  $\nu_6$  ( $K = 1$ ). Supersonic jet combination band data in the near-IR,<sup>15,16</sup> now provides a significantly larger body of information on the intermolecular mode specificity of the tunneling splitting in HF-stretch excited states than available in the ground HF-stretching states. In interpreting these data, one must take into account that there can be both *intra*- and *intermolecular* contributions to the observed tunneling splitting in near-IR combination states, which makes isolating the intermolecular dependence more difficult. Indeed, considerable theoretical effort<sup>10,32,38,39,47,57,60-64</sup> has centered on the correct dynamical interpretation for the threefold reduction in the tunneling splitting between the ground and H(D)F-stretch excited states ( $\nu_1$  and  $\nu_2$ ) in both HF and DF dimer. To a reasonable approximation, however, the intermolecular dependence of the tunneling splitting can be isolated by comparing the combination states (i.e.,  $\nu_1+\nu_x$  or  $\nu_2+\nu_x$ ) with the corresponding  $\nu_1$  and  $\nu_2$  excited states.

Previous combination band studies of the “low frequency” ( $<200\text{ cm}^{-1}$ ) intermolecular modes in  $(\text{HF})_2$  have shown that both  $\nu_4$  and  $\nu_5$  excitation greatly increase (approximately 8-15 fold) the tunneling splitting in HF-stretch excited states. These two low frequency degrees of freedom appear to be strongly mixed

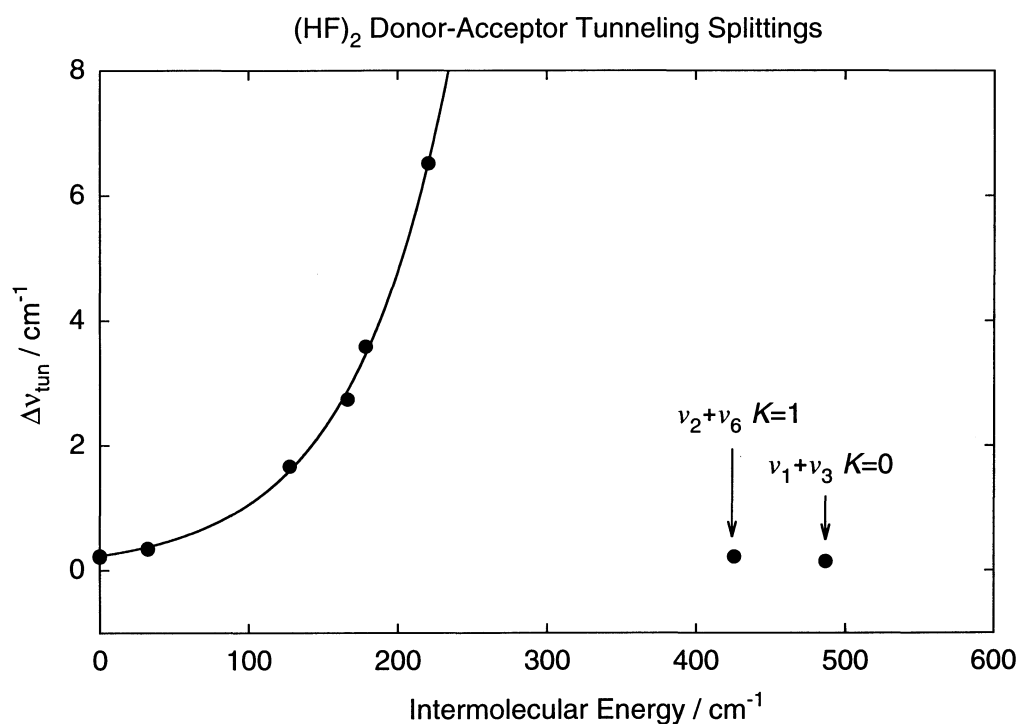


Figure 6.4 Plot of all the observed tunneling splittings in the intermolecular excited combination states versus intermolecular energy. The “low” energy  $\nu_4$  and  $\nu_5$  intermolecular excited states show a dramatic increase in the observed tunneling splitting while the “high” energy  $\nu_3$  and  $\nu_6$  intermolecular excited states do not. This is one indication that both  $\nu_3$  and  $\nu_6$  do not strongly correlate with the tunneling coordinate in (HF)<sub>2</sub>.

Table 6.3 Experimental and theoretical tunneling splittings (cm<sup>-1</sup>) of (HF)<sub>2</sub> in

excited intermolecular states in the ground,  $\nu_1$  and  $\nu_2$  HF-stretching manifolds for both  $K = 0, 1$ .

vib.	$K$	ground state		$\nu_1$		$\nu_2$	
		Expt.	Theory <sup>a</sup>	Expt.	Theory <sup>b</sup>	Expt.	Theory <sup>b</sup>
g. s.	0	0.658690(1) <sup>c</sup>	0.44	0.2155(3) <sup>d</sup>	0.128	0.2334(4) <sup>d</sup>	0.089
g. s.	1	1.064437(1) <sup>d</sup>	0.86	0.3499(1) <sup>d</sup>	----	0.3411(9) <sup>d</sup>	----
$\nu_3$	0	----	15.02	0.1447(4)	----	----	----
$\nu_4$	0	----	0.98	1.6640(2)	0.796	----	0.41
$\nu_5$	0	----	7.48	2.7391(11)	2.283	3.5868(9)	2.028
$\nu_5$	1	----	18.65	----	----	6.5153(13)	----
$\nu_6$	0	----	1.75	----	----	----	----
$\nu_6$	1	1.626(1)	----	----	----	0.2203(6)	----

<sup>a</sup>. Reference 45, 46

<sup>b</sup>. Reference 47

<sup>c</sup>. Reference 8,38

<sup>d</sup>. Reference 10

in HF dimer, with both  $\nu_4$  and  $\nu_5$  having appreciable “geared bend” character.

Interestingly, this appears not to be true for the modes in DF dimer, and thus must be a function not only of coupling in the potential but also vibrational near resonances. As a consequence, the tunneling rates in HF dimer for these two low frequency vibrations are relatively mode-insensitive, and instead depend predominantly on the *total* intermolecular energy and the barrier to interconversion. As discussed in detail in the previous chapter, the energy dependence of the tunneling rates for  $\nu_4$  and  $\nu_5$  can be remarkably well characterized by a simple 1-D tunneling model and a WKB analysis of the tunneling splittings (see Figure 6.4).

In sharp contrast to these results for the low frequency intermolecular

modes, both  $\nu_6$  and  $\nu_3$  excitation do not increase the tunneling splitting significantly. This behavior is demonstrated in Figure 6.4, where all the tunneling splittings measured in HF-stretch excited states are plotted as a function of intermolecular energy; the relevant values are also summarized in Table 6.3. The tunneling splittings measured for both  $\nu_3$  or  $\nu_6$  obviously do not follow the simple WKB extrapolations for the  $\nu_4$  and  $\nu_5$  modes. This data suggests that the vibrational motion associated with these high frequency  $\nu_3$  and  $\nu_6$  modes has very little projection along the most effective tunneling pathway. Alternatively, the small tunneling splittings for  $\nu_3$  and  $\nu_6$  provide particularly strong evidence that the tunneling flux occurs primarily through the low energy “geared” transition state of the PES, rather than over some linear combination of geared, anti-geared, and out-of-plane barriers.

The strong *intermolecular* mode specificity of the tunneling splitting observed in  $(\text{HF})_2$  in the HF-stretch excited states is clearly the predominant effect, yet there is also evidence for a more subtle additional dependence on *intramolecular* excitation as well. For example,  $\nu_6$  excitation ( $K = 1$ ) in the ground HF-stretching state *increases* the tunneling splitting approximately 1.5-fold, while in the  $\nu_2$  excited state,  $\nu_6$  excitation ( $K = 1$ ) *decreases* the tunneling splitting by nearly the same factor. A simple physical model for such an effect could arise from intermolecular  $V \rightarrow V$  transfer between the vibrationally excited tunneling subunits, which if mediated by some near resonant electrostatic (e.g. dipole-dipole) interaction, would be slowed by the presence of a node in the

planar configuration for  $\nu_6$  out-of-plane excitation. In any event, the experimental observations clearly indicate that while the intermolecular dependence can be *approximately* isolated by comparing the tunneling splittings in combination states with the corresponding  $\nu_1/\nu_2$  states, this separation is *not* rigorous and the exact tunneling dynamics depend on all 6 internal degrees of freedom. Further evidence of such a coupled inter/intramolecular dependence to the tunneling rates is also found in corresponding spectroscopic studies of the combination states  $(DF)_2$ , as reported in detail in Chapter VIII.<sup>65</sup>

The tunneling splittings in combination states provide a stringent test of the intra-intermolecular dependence of the full 6-D potential surface, particularly in the region of the barrier to interconversion. Quantitative predictions for tunneling splittings in states that include at least one quantum of HF-stretch excitation are computationally demanding, since it requires accurate quantum calculations of vibrationally metastable “resonance states” at energies substantially above the dissociation limit. Nevertheless, Zhang and coworkers<sup>66</sup> have recently succeeded in performing full 6-D quantum DVR resonance calculations of the energy levels in HF-stretch excited states of  $(HF)_2$ , based on the SQSBDE potential of Quack and Suhm.<sup>39</sup> The results, shown in Table 6.3, indicate that many of the tunneling splitting trends in HF-stretch excited states are qualitatively reproduced, but the calculated tunneling splittings consistently underpredict (by 15%-60%) the corresponding experimental values. Furthermore, the predicted tunneling splittings in the  $\nu_1$  excited states are systematically *larger*

than the analogous levels in the  $\nu_2$  manifold, contrary to experimental findings (see Table 6.3). At least for the two low frequency intermolecular modes,  $\nu_4$  and  $\nu_5$ , the intermolecular dependence of the tunneling splitting in  $(\text{HF})_2$  is qualitatively well reproduced. This may be partially fortuitous, however, since the SQSBDE surface does not appear to correctly reproduce the strength of stretch-bend coupling experimentally observed in  $(\text{HF})_2$ .

An even more significant discrepancy between experiment and theory exists for the tunneling splitting in the  $\nu_3$  anti-gear bend state. Analogous 6-D bound state calculations<sup>46</sup> for the ground HF-stretching states (Table 6.3) predict a 34-fold *increase* in the tunneling splitting in the  $\nu_3$  anti-gear bend fundamental state. This is dramatically different, both in magnitude and direction, from the 1.49-fold *decrease* observed between  $\nu_{1+\nu_3}$  and  $\nu_1$ . This would suggest that the strong enhancement in the tunneling rate predicted by quantum calculations for  $\nu_3$  is incorrect and results from inaccuracies in the PES's along the anti-gear bend coordinate. This interpretation is further supported by disagreement between experimental and predicted  $\nu_3$  intermolecular frequencies, which will be discussed in more detail in Section 6.4.3.

## 6.4.2 Vibrational predissociation

Previous studies of the “geared bend” and “van der Waals stretch” modes indicate that the predissociation rates from combination band excited states are

dominated by the *intramolecular* mode, with a much weaker dependence on *intermolecular* mode as well. Indeed, due to the large difference in the predissociation broadening for  $\nu_2$  (330 MHz) and  $\nu_1$  (10 MHz), this intuition often proved quite useful in confirming assignments of the intramolecular component of combination bands. The two combination bands probed in this study have nearly  $500\text{ cm}^{-1}$  of initial intermolecular excitation, which is at least 2-fold more intermolecular energy than any of the previous low frequency combination bands observed and allows us to sample the intermolecular mode dependence of the predissociation rate at considerably higher energies.

The predissociation lifetimes are determined from a Voigt deconvolution of the HF dimer VRT linewidths. The resulting Lorentzian component from such an analysis can be ascribed completely to predissociation broadening ( $\Delta\nu_{\text{pd}}$ ), since the factors such as pressure and power broadening are negligible for the greatly suppressed collision frequencies in a supersonic jet and typical (<10 mW) difference frequency power levels.<sup>67</sup> The Gaussian component for each transition arises from residual Doppler broadening in the planar expansion, and is determined from an unconstrained least squares fit (floating both Gaussian and Lorentzian components) to selected strong transitions in the  $\nu_2+\nu_6$   $K = 1\leftarrow 0$  band. For the weaker  $\nu_1+\nu_3$   $K=0\leftarrow 0$  combination band observed under identical slit jet conditions, this Gaussian component is scaled linearly by the small (2.9%) fractional change in origins of the  $\nu_1+\nu_3$  and  $\nu_2+\nu_6$  combination bands. High resolution scans (7.5 MHz step size, signal averaging 4-6 pulses of the slit jet)

### Predissociation Broadening in $(\text{HF})_2$ Combination States

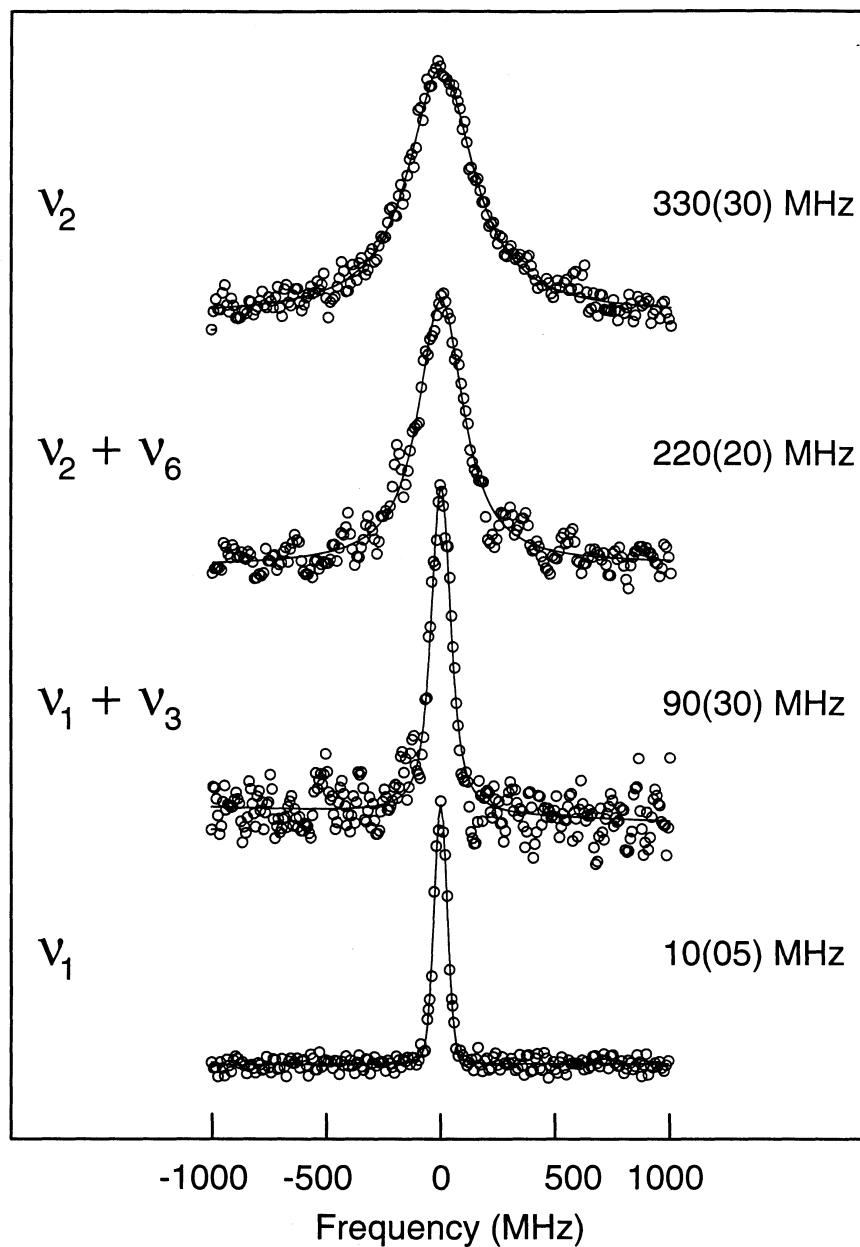


Figure 6.5 Four representative rovibrational lineshapes for both intramolecular fundamentals ( $\nu_1$ ,  $\nu_2$ ), and the  $\nu_2+\nu_6$  and  $\nu_1+\nu_3$   $(\text{HF})_2$  combination bands. The circles are the experimental data, and the lines are the simulated Voigt profiles which deconvolute the inhomogeneous and homogeneous (lifetime) contributions to the broadening. The reported values,  $\Delta\nu_{\text{pd}}$ , are inversely proportional to the lifetime of the excited state. The mode specificity first observed in the intramolecular fundamentals is predominately maintained in the combination bands, however there are also clear effects due to the  $\nu_3$  or  $\nu_6$  excitation on the predissociation broadening.

over transitions for several  $J$  levels in a given VRT band are fit separately. No statistically significant  $J$ -dependence is found in any of the VRT bands studied; the Lorentzian components reported in Table 6.4 therefore represent an average over transitions into several  $J$  states observed in a given VRT band.

The predissociation linewidths for  $\nu_2+\nu_6$  and  $\nu_1+\nu_3$  are very close to the linewidths for  $\nu_2$  and  $\nu_1$ , respectively (see Table 6.4). Nonetheless, a smaller effect due to initial intermolecular excitation is also observed and closely follows a trend first identified in the combination bands associated with  $\nu_4$  and  $\nu_5$ ; intermolecular excitation *increases* predissociation rates in  $\nu_1$  and *decreases* these rates in  $\nu_2$ . Specifically, the predissociation broadening for the two tunneling states of  $\nu_1+\nu_3$  are nearly 10-fold greater than the predissociation broadening in  $\nu_1$ , whereas the predissociation linewidths for both tunneling components of  $\nu_2+\nu_6$  are 25% smaller than the analogous linewidths in  $\nu_2$  (the  $\nu_2$   $K=1$  predissociation rates have not yet been measured). This is particularly evident in Figure 6.5, which shows representative lineshapes for the  $\nu_2+\nu_6$  and  $\nu_1+\nu_3$  combination bands along with the  $\nu_1$  and  $\nu_2$  fundamentals. The strong  $\nu_1/\nu_2$  mode specific predissociation rates are evident by comparing the fundamental lineshapes in Figure 6.5, but the weaker effect of intermolecular excitation is also clearly visible.

This intermolecular dependence of the predissociation broadening suggests the following interpretation. In the absence of intermolecular excitation, the two intramolecular modes are best described as nearly local modes with the vibrational

energy either in the “free” or “bound” HF subunit. Consequently, these two vibrations can have dramatically different predissociation rates with  $\nu_2$  (predominately “bound”) predissociating 30-50 fold faster than  $\nu_1$  (predominately “free”).<sup>13</sup> Indeed, it has been postulated that predissociation only occurs from the “bound” HF-stretch, and thus the difference in predissociation rates is a measure of the local mode character of the two intramolecular modes.<sup>61</sup> Intermolecular excitation, however, tends to weaken the hydrogen bonding interactions that make  $\nu_1$  distinct from  $\nu_2$ . Therefore, small changes in the “bound” vs. “free” character of the two intramolecular modes induced by intermolecular excitation can lead to large fractional differences in the observed predissociation rates from combination states.

From a theoretical perspective, Zhang, Bacic and coworkers<sup>68</sup> have presented 4-D time independent golden rule calculations of the vibrational predissociation lifetimes for  $(\text{HF})_2$  on the SQSBDE surface. Initial calculations for  $\nu_1$  and  $\nu_2$  have recently been extended to combination states<sup>69</sup> of the intramolecular modes with  $\nu_4$  and  $\nu_5$ ; all these results are also shown in Table 6.4. The qualitative agreement between experiment and theory is quite good, i.e., the calculated values do reproduce the broader predissociation widths for  $\nu_2$  vs.  $\nu_1$  excitation. In addition, the increased broadening in the  $\nu_1+\nu_4$  and  $\nu_1+\nu_5$  combination states relative to the  $\nu_1$  state, and decreased broadening between the  $\nu_2+\nu_5$  and  $\nu_2$  states are also correctly predicted. However, the trend between  $\nu_2+\nu_4$  and  $\nu_2$  is not well reproduced, i.e., the  $\nu_2+\nu_4$  predissociation linewidth is broader

Table 6.4 Vibrational predissociation linewidths (MHz) for HF dimer. The A<sup>+</sup> and B<sup>+</sup> symmetry labels refer to  $\Gamma_{\text{vib-tun}}$  in the upper vibrational state.

$\Gamma_{\text{vib-tun}} =$	$\Delta v_{\text{pd}} / \text{MHz}$			
	Expt		Theory <sup>a</sup>	
	A <sup>+</sup>	B <sup>+</sup>	A <sup>+</sup>	B <sup>+</sup>
$\nu_1$	6.4(5) <sup>b</sup>	9.5(5) <sup>b</sup>	4.9	4.1
$\nu_1 + \nu_3$	90(20)	60(20)	----	----
$\nu_1 + \nu_4$	25(5)	40(8)	8.2	12
$\nu_1 + \nu_5$	20(5)	45(8)	5.2	5.5
$\nu_1 + \nu_6^c$	----	----	----	----
$\nu_2$	330(30) <sup>b</sup>	330(30) <sup>b</sup>	48	51
$\nu_2 + \nu_3$	----	----	----	----
$\nu_2 + \nu_4$	----	300(50)	85	83
$\nu_2 + \nu_5$	270(20)	270(20)	29	38
$\nu_2 + \nu_6^c$	240(20)	250(20)	----	----

<sup>a.</sup>  $\Delta v_{\text{pd}}$  is calculated using the predissociation lifetimes reported in Refs 68,69.

<sup>b.</sup> Reference 13

<sup>c.</sup> The  $\nu_6$  states are odd parity so the symmetry labels are  $\Gamma_{\text{vib-tun}} = \text{A}^-$  and  $\text{B}^-$ , respectively.

than  $\nu_2$ , in clear disagreement with experiment. At a more quantitative level of comparison, the predicted predissociation linewidths are systematically too small, typically a factor of 2-8 smaller than the experimental value. Extension of these vibrational predissociation calculations to  $\nu_1 + \nu_3$  and  $\nu_2 + \nu_6$  would be useful since these two modes display larger intermolecular effects on the predissociation broadening. It also would be interesting to examine the intramolecular dependence of the eigenfunctions calculated in the 6-D resonance state calculations<sup>46</sup> to determine if the present interpretation that the changes in the predissociation rates in combination states result from changes in the

intramolecular local mode character of  $\nu_1$  and  $\nu_2$ . Indeed, vibrational predissociation calculations provide a demanding test of the accuracy of the potential, in particular for the anisotropy of the repulsive wall and the coupling between inter- and intramolecular degrees of freedom. The present predissociation calculations suggest that the SQSBDE surface does a reasonably good job at capturing predissociation trends, though it considerably underpredicts the magnitude of inter/intramolecular mode coupling.

### 6.4.3 Extrapolation to intermolecular vibrational frequencies

One of the primary goals of the present study is to provide detailed high resolution measurements for *all* intermolecular degrees of freedom in a prototypic hydrogen bonded complex. Since the current study necessarily observes these vibrations via combination bands built on high frequency intramolecular HF-stretching modes, the most direct and rigorous comparison with theory would be via full 6-D “resonance” calculations on exactly these combination states. However, these resonance calculations are quite demanding and, furthermore, can not isolate discrepancies due to inter vs. intramolecular regions of the potential surface. Thus, a more useful alternative strategy would be to develop a procedure for extrapolating intermolecular frequencies from the available combination band data to the ground (i.e.,  $\nu_1/\nu_2 = 0$ ) state, in essence, predicting the vibrational frequencies that would be observed in a far-IR experiment. Basically, this

amounts to a relatively small correction for off-diagonal anharmonicity between the inter- and intramolecular degrees of freedom. These results can then be compared with *exact* 6-D calculations on a trial potential surface for intermolecular modes *without*  $\nu_1/\nu_2$  excitation, and thereby probe the intermolecular dependence of the potential surface in near isolation.

To make improved predictions of the  $\nu_3$  and  $\nu_6$  *fundamental* frequencies from *combination* band data, we take advantage of the strong correlation between (i) the intermolecular frequency determined from neglecting off-diagonal anharmonicity (i.e.,  $\nu_{\text{comb}} = \nu_{\text{intra}} + \nu_{\text{inter}}$ ) and (ii) the intramolecular redshift of the HF-stretching mode on which the combination band is built. Physically, this nearly linear correlation arises because these redshifts are a direct measure of the small increase in hydrogen bond strength upon  $\nu_1/\nu_2$  excitation, which in turn slightly increases the intermolecular vibrational frequencies. Indeed, this correlation has been shown to be remarkably good for  $\nu_4$  and  $\nu_5$  in (HF)<sub>2</sub>, as well as for the corresponding intermolecular modes in (DF)<sub>2</sub>. Furthermore, where this can be tested, the fractional intermolecular frequency shift in (HF)<sub>2</sub> and (DF)<sub>2</sub> proves to be largely independent of the intermolecular mode.

This motivates the following simple model, whereby the set of all near-IR measurements for which intermolecular frequencies are obtained from both  $\nu_1$  and  $\nu_2$  combination bands are least squares fit to a single parameter expression,

### Extrapolation to $(\text{HF})_2$ Intermolecular Fundamental Frequencies

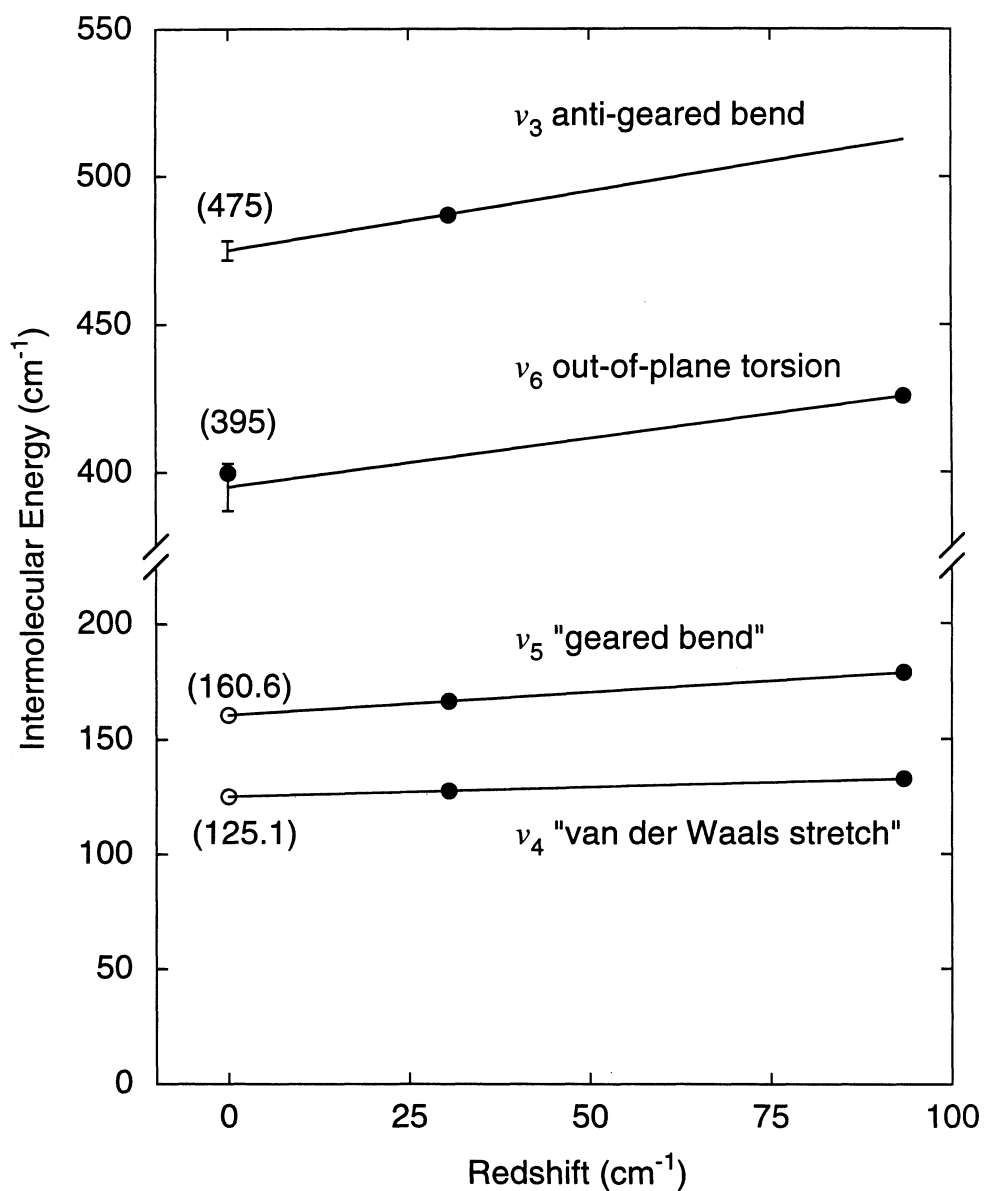


Figure 6.6 Plot of all the measured (filled circles) intermolecular energies as a function of intramolecular redshift. Both the  $\nu_4$  and  $\nu_5$  energies have been reported previously and were used to make extrapolations (see text for details) of the far-IR (zero redshift) intermolecular energies of  $\nu_3$  ( $K = 0$ ) and  $\nu_6$  ( $K = 1$ ).

$$\frac{E_{\text{inter}}^{\nu_{1,2}} - E_{\text{inter}}^{\text{g.s.}}}{E_{\text{inter}}^{\text{g.s.}}} = b(\nu_{\text{HF}} - \nu_{1,2}) \quad (6.2)$$

In Eq (6.2),  $E_{\text{inter}}^{\nu_{1,2}}$  is the intermolecular energy determined from the  $\nu_1$  or  $\nu_2$  combination band and  $E_{\text{inter}}^{\text{g.s.}}$  is the intermolecular frequency in the ground HF - stretching state (i.e., for zero redshift). The results of this model are plotted in Figure 6.6 and presented in Table 6.5 for all four intermolecular modes, and, where comparison data is available, indicate essentially quantitative agreement with experiment. For example, the  $395(8) \text{ cm}^{-1}$  value for  $\nu_6$  ( $K = 1$ ) obtained from the model extrapolation agrees with far-IR experimental measurement of  $399.787(1) \text{ cm}^{-1}$  to well within the uncertainty of the fit, suggesting this as a useful algorithm for predicting far-IR intermolecular frequencies for a high resolution spectral search.

In the case of the  $\nu_3$  anti-g geared bend mode, extrapolation of the combination band data leads to a  $J = K = 0$  value of  $475(3) \text{ cm}^{-1}$  (the smaller uncertainty in this estimate for  $\nu_3$  is due to the fact that the experimental near-IR value is from a  $\nu_1$  based combination band with a 2-3 fold smaller redshift). This is the only intermolecular mode for which neither far-IR nor near-IR data had been previously available, and thus completes the set of 4 intermolecular modes. For both the  $\nu_4$  and  $\nu_5$  vibrations, reliable values already exist for the  $J = K = 0$  energies; as evident in Figure 6.6, the agreement between experimental the far-IR results and the values predicted from Eq. (6.2) is excellent. The  $\nu_6$  out-of-plane intermolecular mode can only be observed in perpendicular bands in both the far

Table 6.5 Intermolecular energies ( $J=K$ ) determined from the near-IR combination bands. The ground state HF-stretching frequencies are the extrapolated predictions of the intermolecular fundamentals. The results of exact 6-D quantum calculations for two high quality (HF)<sub>2</sub> PES's are also included for comparison. All values are in cm<sup>-1</sup>.

vib.	$K$	$\nu_2$	$\nu_1$	Extrapolated	far-IR	SQSBDE <sup>a</sup>	BJKLK <sup>b</sup>
$\nu_3$	0	-----	487.0153(4)	475(3)		425.30	430.29
$\nu_4$	0	132.6160(19)	127.5726(2)	125.1(1)	125(5) <sup>c</sup>	126.37	123.59
$\nu_5$	0	178.6673(4)	166.5232(2)	160.6(6)	161(5) <sup>d</sup>	160.58	163.37
$\nu_6$	0	-----	-----		375(5) <sup>e</sup>	378.72	380.76
$\nu_6$	1	425.6897(5)	-----		399.787(1) <sup>e</sup>	402(4) <sup>b</sup>	-----

- a. Reference 46.
- b. Reference 48,49
- c. Reference 39
- d. Reference 8
- e. Reference 6

and near-IR, and thus data is only available for  $K=1$ . The resulting three  $K=0\leftarrow 0$  ( $\nu_3, \nu_4, \nu_5$ ) and one  $K=1\leftarrow 0$  ( $\nu_6$ ) intermolecular frequencies are plotted in Figure 6.7.

Due to the predominant role of large amplitude motion on an anharmonic potential surface any quantitative comparison between theory and experiment requires that the large amplitude intermolecular dynamics be included. The results of such full 6-D calculations on the SQSBDE and BJKLK surface are also reported in Table 6.5. It is apparent that even though the SQSBDE surface was empirically adjusted to reproduce the experimentally observed dissociation energy ( $D_0$ ) of the complex, that the predictions from both potential surfaces are in substantial agreement with one another. However, the dramatic importance of anharmonic corrections in these full 6-D calculations can be appreciated by comparing the harmonic ( $\omega$ ) and anharmonic ( $\nu$ ) intermolecular frequencies both calculated on the SQSBDE surface.

As discussed previously, the frequencies of the  $\nu_4$  and  $\nu_5$  intermolecular vibrations are well reproduced by both sets of 6-D calculations, yet significant discrepancies between experiment and theory have been identified by quantities sensitive not only to the eigenvalue but the eigenfunction as well. In the case of the  $\nu_6$  vibration, only the *excited*  $K=1$  state has been observed, so that the experimental  $\nu_6$  frequency can not be compared directly with the exact 6-D results ( $J=0, K=0$ ). Therefore, comparison is made with 6-D quantum Monte Carlo

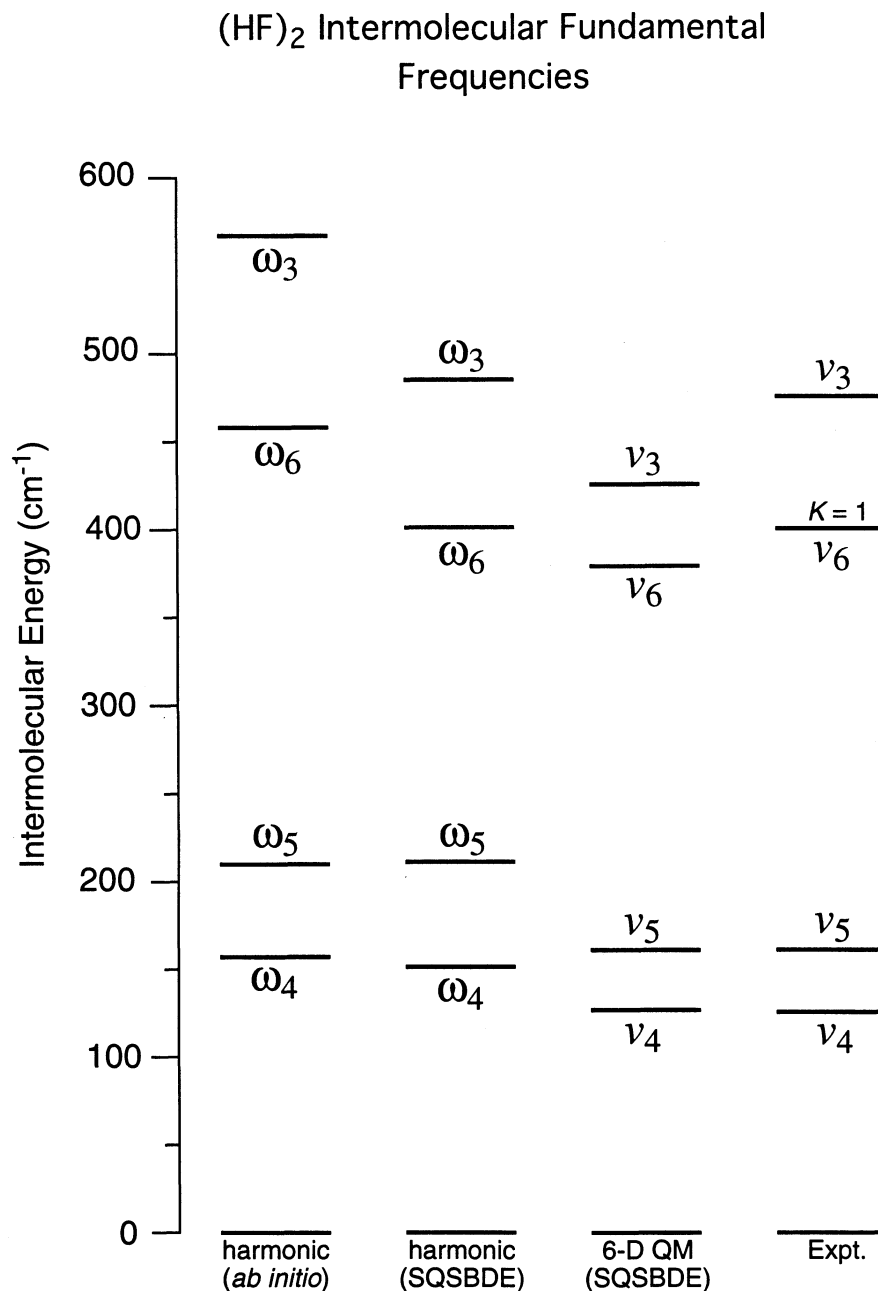


Figure 6.7 The four intermolecular energies of (HF)<sub>2</sub> in the ground HF-stretching state determined from combination bands are compared to two levels of theory. First harmonic estimates of the intermolecular energies based on (i) *ab initio* calculations and (ii) the SQSBDE potential. Second, full 6D calculations on the SQSBDE and BJBKE analytical potential surfaces. Clearly, the harmonic calculations overestimate the experimental energies and thus for quantitative comparison the 6-D QM calculations must be performed. The agreement of the theoretical predictions based on the two potential energy surfaces with experiment is excellent, except for  $\nu_3$  the high frequency anti-gear bend.

calculations performed on the SQSBDE surface which have been approximately extended to excited rotational levels using the clamped coordinate quasiadiabatic channel method.<sup>38</sup> The  $402\text{ cm}^{-1}$  predicted value of  $\nu_6 K = 1$  is in excellent agreement (0.5%) with the far-IR measurements, which suggests that the non-planar part of the PES is modeled with reasonable accuracy. In addition, extrapolated values of  $\nu_6 K = 0$  have been made based on far-IR measurements<sup>39</sup> which allow the rotationless  $\nu_6$  vibration to be estimated at  $375(5)\text{ cm}^{-1}$  (See Table 6.5); this is important for calculating the zero-point energy associated with the intermolecular modes.

The largest discrepancy between theory and experiment is on the frequency of  $\nu_3$  fundamental (see Figure 6.7). The  $475(3)\text{ cm}^{-1}$  value is *underestimated* on both PES's by approximately 10%. This is by far the largest deviation measured for all the intermolecular modes and thus warrants further efforts to identify the possible reason for the failure. For example, the  $\nu_3$  eigenfunction calculated in the 6-D quantum calculations does not have the nodal pattern expected for a pure anti-gear bend, but also has appreciable gear bend character.<sup>46</sup> As discussed previously, this could be due to significant angular-angular and radial-angular coupling in the PES, resulting in partial mixing between anti-gear bend and overtone/combination levels of the gear bend and van der Waals stretch.

This interpretation that the  $\nu_3$  state on the SQSBDE surface has appreciable gear bend character is certainly consistent with the large predicted

increase (34-fold) in the tunneling splitting for this excited intermolecular state. In contrast, the tunneling splitting observed *experimentally* for the  $\nu_1+\nu_3$  state is quite small and does not reflect a large increase relative to the  $\nu_1$  state splitting. The large increases in the tunneling splitting for the lower energy  $\nu_4$  and  $\nu_5$  excited states was interpreted as evidence of appreciable geared bend character for both these state, and thus considerable projection along the tunneling coordinate. The disagreement between theory and experiment for the anti-geared bend energy therefore may result from too much geared bend character in the predicted  $\nu_3$  state, which has the effect of increasing the tunneling splitting and possibly lowering the intermolecular energy. Instead, the  $\nu_3$  experimental data is consistent with a higher energy state that has little or no geared bend character at all.

#### 6.4.4 An empirical estimate of $D_e$

The set of intermolecular fundamental vibrations for  $(\text{HF})_2$  described above can be used to provide a much improved empirical estimate of  $D_e$ . This is a particularly problematic issue in weakly bound systems and highlights the exquisite difficulty of making a detailed comparison between full quantum theory and experiment. Since any spectroscopic measurement obtains differences in experimental eigenvalues, any rigorous comparison necessarily requires that (i) a *global potential surface* be constructed, and (ii) the corresponding multidimensional quantum mechanics be solved exactly on this surface with no dynamical approximation. The first step of generating a global potential surface

from *ab initio* methods is a major challenge, with obvious tradeoffs between quality of calculation per geometry and the number of configurations sampled. However, even given such a global potential surface, this second step is not currently feasible for a hydrogen bonded cluster with more than 4 atoms (such as H<sub>2</sub>O dimer); for a relatively “simple” species such as (HF)<sub>2</sub> with only 2 heavy atoms, this  $3N-6 = 6$  dimensional calculation already represents the state-of-the-art.

A simpler alternative, (at least from a theoretical perspective) is to perform a limited number of much higher level *ab initio* calculations to obtain  $D_e$ , the binding energy of the global minimum with respect to dissociation. For example, there have been recent *ab initio* calculations by both Dunning<sup>70</sup> and Schaefer<sup>71</sup> on (HF)<sub>2</sub>, which provide new values for  $D_e$  treating correlation effects at a level much higher than was possible in the earlier work of Kofranek *et al.*,<sup>30</sup> and on which both the BJKLK and QSBDE analytical surfaces are explicitly based. Since  $D_e$  is not an experimental observable, however, we must use spectroscopic methods to provide quantum corrections to the true experimental observables such as  $D_0$ . The present high resolution combination band data on HF dimer, and in particular the measurement of the  $\nu_3$  antigeared bend, make this possible.

The essential difficulty associated with a spectroscopic determination of  $D_e$  is the amount of zero-point energy associated with the intermolecular modes ( $E_{\text{inter}}$ ). The well depth  $D_e$ , is obtained from the dissociation energy ( $D_0$ ) by

$$D_e = D_0 + E_{\text{inter}} + \Delta E_{\text{intra}} \quad (6.3)$$

where  $E_{\text{inter}}$  is the sum of zero-point energies of the intermolecular vibrations in the dimer, and  $\Delta E_{\text{intra}}$  is the change in the zero-point energy associated with the high frequency HF-stretches. The dissociation energy  $D_0$  of  $(\text{HF})_2$  has been very accurately determined to be  $1062(1) \text{ cm}^{-1}$  by the photofragment studies of Miller and coworkers.<sup>14,72,73</sup> The change in the *harmonic* zero-point energies of the two high frequency HF-stretches upon dimerization can be adequately approximated from the known vibrational frequencies of the dimer and monomer, i.e.,  $\Delta E_{\text{intra}} = [\nu_{\text{HF}} - (\nu_1 + \nu_2)/2] = 61.9313(3) \text{ cm}^{-1}$ . An even better approximation that takes *anharmonic* effects into account is possible, since extensive overtone series have been observed in both the monomer<sup>74,75</sup> and the dimer.<sup>17-19</sup> If one treats the monomer ( $\nu_{\text{HF}}$ ) and dimer (both  $\nu_1$  and  $\nu_2$ ) modes as Morse oscillators, the magnitude of this additional anharmonic term is  $-7.1 \text{ cm}^{-1}$ . This yields a net value for the intramolecular zero-point contributions of  $\Delta E_{\text{intra}} = 54.8 \text{ cm}^{-1}$ , with an uncertainty of at most  $1 \text{ cm}^{-1}$ .

By far the largest correction in obtaining  $D_e$  from  $D_0$  is associated with zero-point energy in the low-frequency intermolecular modes, the frequencies of which have now all been measured or accurately estimated for the ground state. The challenge is to use the experimentally observed fundamental frequencies to predict accurately the amount of intermolecular zero-point energy, which we estimate via the following method. We calculate the 4-D intermolecular zero-

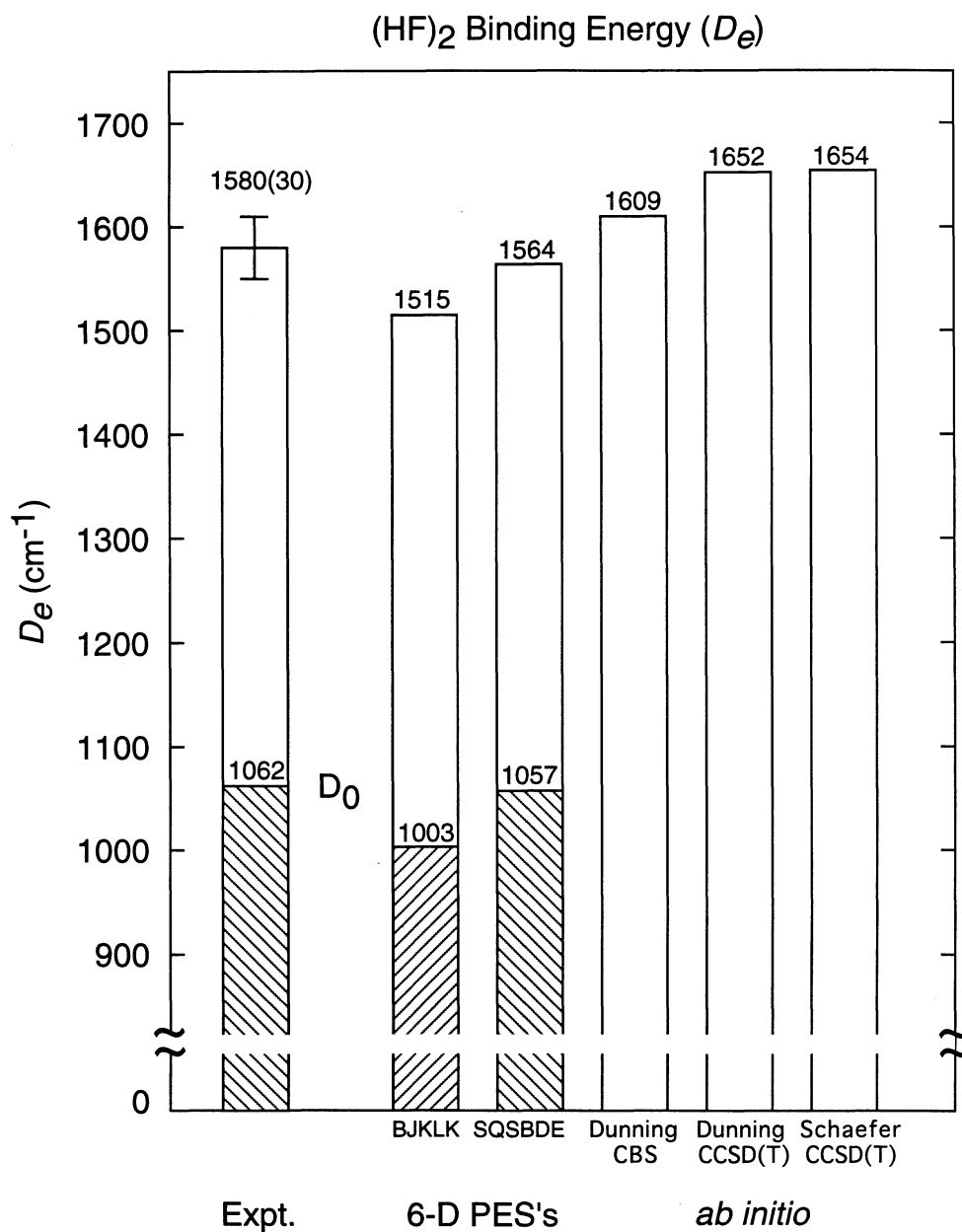


Figure 6.8 A bar chart of the estimates of the dissociation energy ( $D_0$ ) and hydrogen bond energy ( $D_e$ ) of (HF)<sub>2</sub>. The current experimental estimate is compared to semi-empirical estimates based on the 6-D potentials of Bunker et al. and Quack and Suhm along with two recent *ab initio* calculations. The current estimate of  $D_e$  (see text for details) is greater than both semi-empirical estimates and more consistent with the *ab initio* calculations.

point energy directly on a trial potential surface by solving for the energy of the intermolecular ground state with respect to the minimum on the potential. For HF monomers clamped at vibrationally averaged bond lengths ( $r_{\text{HF}} = 1.767 a_0$ ), the calculated intermolecular zero-point energy on the SQSBDE potential is  $E_{\text{inter}}^{\text{theory}} = 547.63 \text{ cm}^{-1}$ . If we then assume that the *ratio* of the true zero-point energy to the sum of the intermolecular fundamental frequencies is adequately reproduced by the SQSBDE surface, the experimental zero-point energy can be obtained from

$$\frac{E_{\text{inter}}^{\text{expt}}}{\sum_i \nu_i^{\text{expt}}} = \frac{E_{\text{inter}}^{\text{theory}}}{\sum_i \nu_i^{\text{theory}}} \quad (6.4)$$

The ratio of the zero-point energy to the sum of 4-D intermolecular frequencies is calculated to be 0.5028 of the SQSBDE surface, leading to an *experimental* estimate of  $E_{\text{inter}}^{\text{expt}} = 5710 \text{ cm}^{-1}$ . For comparison, the BJCLK surface predicts a ratio of 0.5097, but the near quantitative agreement for this ratio on both potentials is more an indication of the similarities between the two surfaces than a measure of the accuracy of this method for predicting the true intermolecular zero-point energy. The experimental value of  $E_{\text{inter}}^{\text{expt}}$  is only slightly larger than the theoretical value calculated on the SQSBDE surface because this surface reproduces 96% of the sum of experimental intermolecular frequencies [see Eq. (6.4)]. Thus our best estimate for  $D_e$  is  $1580(35) \text{ cm}^{-1}$ , where the uncertainty is dominated by the accuracy of the zero-point ratio (0.5028) used to scale the experimental results. We conservatively estimate a possible  $\pm 5\%$  error in this

zero-point ratio based on how well the SQSBDE surface reproduces the sum of intermolecular frequencies. However, this zero-point ratio and the corresponding value of  $D_e$  should be tested and improved as further refinements of the potential surface become available. The  $D_e$  value determined from the present analysis is compared with selected theoretical predictions in Fig. 6.8.

The  $D_e$  values on both the BJKLK and SQSBDE PES's are smaller than the present experimental estimate. These potentials are constructed from the *ab initio* calculations of Kofranek *et al.*<sup>30</sup> using the coupled pair functional method, with additional *ab initio* points added by Bunker *et al.*<sup>28,30</sup> using the closely related averaged coupled pair functional level of theory. The BJKLK surface predicts  $D_e = 1515 \text{ cm}^{-1}$  and  $D_0 = 1003 \text{ cm}^{-1}$ , both of which are significantly lower than experiment. Because it was empirically adjusted to reproduce  $D_0$ , somewhat better agreement is achieved with the SQSBDE surface. However, a closer inspection of the SQSBDE surface reveals the excellent agreement for  $D_e$  is partially fortuitous. In particular, the change in high frequency HF-stretching zero-point energy is underestimated<sup>76</sup> on the SQSBDE potential [ $\Delta E_{\text{intra}} \approx 3958 - (3940.6 + 3896.4)/2 = 39.5 \text{ cm}^{-1}$ ] by nearly  $22 \text{ cm}^{-1}$  while the intermolecular zero-point energy is also approximately  $23 \text{ cm}^{-1}$  ( $571.0 - 547.6 \text{ cm}^{-1}$ ) too small. Thus, on the SQSBDE surface these two errors nearly cancel [see Eq. (6.3)], leaving the predicted value of  $D_e$  within 1% of experiment. This difficulty in correctly modeling the intra/intermolecular dependence of the full 6-D potential is fully appreciated by the authors of the SQSBDE surface,<sup>77</sup> and indeed is the focus of

current efforts to generate improved semiempirical (HF)<sub>2</sub> potentials.

Recently, Peterson and Dunning reported the geometry and hydrogen bond energy of (HF)<sub>2</sub> using several theoretical methods including Moller-Plesset perturbation and coupled cluster theories with large correlation consistent basis sets.<sup>70</sup> They also investigated the effect of basis set superposition error on the (HF)<sub>2</sub> binding energy using the standard counterpoise (CP) correction method.<sup>78</sup> The CP corrected  $D_e$  values are consistently lower than the uncorrected values for a given basis set, but these differences decrease regularly with increasing quality of the basis set. At their highest level of theory using coupled clusters singles and doubles with perturbative estimate of triple excitations [CCSD(T)] and the largest basis set, the CP corrected (uncorrected) value of  $D_e$  is 1564 cm<sup>-1</sup> (1652 cm<sup>-1</sup>). However, Peterson and Dunning have taken these calculations one step further; from the systematic dependence of  $D_e$  on increasing the quality of the basis set, extrapolation to the “complete” basis set limit (CBS) predicts  $D_e = 4.60$  kcal/mol = 1610 cm<sup>-1</sup> (See Figure 6.8). Thus for the CCSD(T) calculations the CP corrected  $D_e$  values approach the CBS limit from below while the uncorrected values approach it from above, yet as they should, both predict the same CBS limit. This is now in good agreement with experiment, yet is still on the high side of the stated uncertainty in  $D_e$  and in principle may indicate some small residual discrepancy. Nevertheless, the agreement between *ab initio* theory and experiment is already verified on the < 0.1 kcal/mol level, which in the field of hydrogen bonding interactions represents a significant accomplishment.

In a later *ab initio* study by Schaefer and coworkers<sup>71</sup> at the CCSD(T) level of theory using similarly large basis sets,  $D_e$  was predicted to be 1654  $\text{cm}^{-1}$  without CP correction, i.e., well within 0.01 kcal/mol of the comparable prediction of Peterson and Dunning. These calculations were not corrected for basis set superposition error so further comparison of  $D_e$  with experiment is not possible. However, Schaefer and coworkers presented harmonic vibrational frequencies and IR intensities using the CCSD(T) method and a series of large basis sets. These calculations predict  $\omega_6$  and  $\omega_3$  at *higher* frequencies than the corresponding harmonic predictions on the SQSBDE surface (the  $\omega_4$  and  $\omega_5$  predictions are nearly identical to the SQSBDE values, see Figure 6.7). As discussed earlier, harmonic predictions of the intermolecular modes can not be quantitatively compared with experiment, but a prediction of the anharmonic frequencies for the new *ab initio* calculations can be made if the harmonic frequencies are scaled by the  $\omega_{ex}/\omega_e$  ratios calculated on the SQSBDE surface. With this procedure to scale the Schaeffer results,  $\nu_3$  is predicted at 507(10)  $\text{cm}^{-1}$  and  $\nu_6$  at 436(10)  $\text{cm}^{-1}$ . This value of  $\nu_6$  is significantly greater (16%) than the experimentally extrapolated value (see Table 6.5), which may reflect inaccuracies in the *ab initio* results. The value of  $\nu_3$  on the other hand is in much better agreement (4%) with the experimental value than either of the  $\nu_3$  frequencies calculated on the analytical surfaces (-10%).

As a final test of potential surfaces, one area that deserves further theoretical investigation is the prediction of IR intensities in  $(\text{HF})_2$ . For example,

early 4-D quantum calculations of far-IR intensities in (HF)<sub>2</sub> by Clary and coworkers<sup>59</sup> based on the BJKLK potential surface predict the  $\nu_3$  anti-gear bend to be a factor of 15 weaker than the  $\nu_5$  geared bend in oscillator strength. This prediction of a weaker  $\nu_3$  vs.  $\nu_5$  mode is actually in good qualitative agreement with experiment ( $I_{\text{geared}}/I_{\text{anti-gear}} = 17$ ), whereas the most sophisticated *ab initio* calculations predict that  $\nu_3$  is 1.13-fold *stronger* than the  $\nu_5$  geared bend.<sup>71</sup> In addition, several of the intermolecular modes are observed in combination with *only one* of the intramolecular modes, e.g.  $\nu_2 + \nu_6$  is quite strong but  $\nu_1 + \nu_6$  must be down in oscillator strength by at least 200 fold to avoid detection at our current sensitivities. Theoretical predictions of combination band intensities using the 6-D quantum methods may provide insight into the intensity anomalies identified in (HF)<sub>2</sub>. These types of *eigenfunction* sensitive calculations would provide particularly demanding tests of the current hydrogen bond potentials. Furthermore, since intra-intermolecular coupling plays a key role in determining the transition strength of combination bands, such calculations and comparisons offer a crucial level of information to construct the next generation of (HF)<sub>2</sub> potential surfaces.

## 6.5 Summary

In this chapter, we report the measurement of near infrared VRT spectra for (HF)<sub>2</sub> which access excited states in both the out-of-plane torsion and anti-gear bend coordinates for excited HF-stretch vibrational states. The donor-

acceptor tunneling splitting is not strongly increased in the  $\nu_3$  or  $\nu_6$  intermolecular excited states, which indicates that neither of these two intermolecular modes is significantly coupled with the tunneling coordinate. Predissociation broadening in the combination bands is dominated by intramolecular mode specificity, yet there is also an appreciable dependence on the intermolecular mode as well. This is qualitatively consistent with a simple physical model of the influence of intermolecular excitation on the mixing between the “free” and “bound” HF-stretch character of the intramolecular modes.

With the observation of  $\nu_2+\nu_6$  and  $\nu_1+\nu_3$ , all four intermolecular modes have now been detected in the near-IR via combination bands. The near-IR data have been used to make predictions of the intermolecular fundamental frequencies, which in turn permit a careful evaluation of the current potentials. Excellent agreement is found for all the intermolecular frequencies except for the anti-g geared bend which is under predicted (10%) by 6-D quantum calculations. Similarly, the tunneling splittings for intermolecular excited states are well predicted except for the  $\nu_3$  excited state. In addition, knowledge of all four intermolecular modes in  $(\text{HF})_2$  permit the hydrogen bond energy ( $D_e$ ) to be experimentally estimated at  $1580(35) \text{ cm}^{-1}$  ( $4.52(10) \text{ kcal/mol}$ ). Agreement with recent high level *ab initio* calculations of  $D_e$  is within the  $35 \text{ cm}^{-1}$  ( $0.1 \text{ kcal/mol}$ ) experimental uncertainty. However, these high level *ab initio* calculations have thus far only been performed for a limited range of dimer geometries near equilibrium. It remains an outstanding question and challenge whether a

sufficiently dense grid of points can be obtained at this level of theory, which would stimulate the development of a significantly improved “benchmark” potential surface for this prototypic hydrogen bonded system.

## References for Chapter 6

- 1 T. R. Dyke, B. J. Howard, and W. Klemperer, *Journal of Chemical Physics* **56**, 2442 (1971).
- 2 W. J. Lafferty, R. D. Suenram, and F. J. Lovas, *Journal of Molecular Spectroscopy* **123**, 434 (1987).
- 3 B. J. Howard, T. R. Dyke, and W. Klemperer, *Journal of Chemical Physics* **81**, 5417 (1984).
- 4 H. S. Gutowsky, C. Chuang, J. D. Keen, T. D. Klots, and T. Emilsson, *Journal of Chemical Physics* **83**, 2070 (1985).
- 5 K. von Puttkamer and M. Quack, *Molecular Physics* **62**, 1047 (1987).
- 6 K. von Puttkamer, M. Quack, and M. A. Suhm, *Molecular Physics* **65**, 1025 (1988).
- 7 K. von Puttkamer and M. Quack, *Chemical Physics* **139**, 31 (1989).
- 8 M. Quack and M. A. Suhm, *Chemical Physics Letters* **171**, 517 (1990).
- 9 A. S. Pine and W. J. Lafferty, *Journal of Chemical Physics* **78**, 2154 (1983).
- 10 A. S. Pine, W. J. Lafferty, and B. J. Howard, *Journal of Chemical Physics* **81**, 2939 (1984).
- 11 R. L. DeLeon and J. S. Muentzer, *Journal of Chemical Physics* **80**, 6092 (1984).
- 12 A. S. Pine and B. J. Howard, *Journal of Chemical Physics* **84**, 590 (1986).
- 13 A. S. Pine and G. T. Fraser, *Journal of Chemical Physics* **89**, 6636 (1988).
- 14 E. J. Bohac, M. D. Marshall, and R. E. Miller, *Journal of Chemical Physics* **96**, 6681 (1992).
- 15 E. J. Bohac and R. E. Miller, *Journal of Chemical Physics* **99**, 1537 (1993).

- 16 D. T. Anderson, S. Davis, and D. J. Nesbitt, *Journal of Chemical Physics* **104**, 6225 (1996).
- 17 M. A. Suhm, J. T. Farrell, Jr., A. McIlroy, and D. J. Nesbitt, *Journal of Chemical Physics* **97**, 5341 (1992).
- 18 H.-C. Chang and W. Klemperer, *Journal of Chemical Physics* **98**, 9266 (1993).
- 19 H.-C. Chang and W. Klemperer, *Journal of Chemical Physics* **100**, 1 (1994).
- 20 D. R. Yarkony, S. V. O'Neil, H. F. Schaefer III, C. P. Baskin, and C. F. Bender, *Journal of Chemical Physics* **60**, 855 (1974).
- 21 A. E. Barton and B. J. Howard, *Faraday Discuss. Chem. Soc.* **73**, 45 (1982).
- 22 J. F. Gaw, Y. Yamaguchi, M. A. Vincent, H. F. Schaefer III, C. P. Baskin, and C. F. Bender, *J. Am. Chem. Soc.* **106**, 3133 (1984).
- 23 D. W. Michael, C. E. Dykstra, and J. M. Lisy, *Journal of Chemical Physics* **81**, 5998 (1984).
- 24 D. W. Schwenke and D. G. Truhlar, *Journal of Chemical Physics* **82**, 2418 (1985).
- 25 M. J. Frisch, J. E. Del Bene, J. S. Binkley, and H. F. Schaefer III, *Journal of Chemical Physics* **84**, 2279 (1986).
- 26 J. E. Del Bene, *Journal of Chemical Physics* **86**, 2110 (1987).
- 27 M. J. Redmon and J. S. Binkley, *Journal of Chemical Physics* **87**, 969 (1987).
- 28 P. R. Bunker, M. Kofranek, H. Lischka, and A. Karpfen, *Journal of Chemical Physics* **89**, 3002 (1988).
- 29 G. C. Hancock, D. G. Truhlar, and C. E. Dykstra, *Journal of Chemical Physics* **88**, 1786 (1988).
- 30 M. Kofranek, H. Lischka, and A. Karpfen, *Journal of Chemical Physics* **121**, 137 (1988).

- 31 D. W. Schwenke and D. Truhlar, G., *Journal of Chemical Physics* **88**, 4800 (1988).
- 32 P. R. Bunker, T. Carrington, Jr., P. C. Gomez, M. D. Marshall, M. Kofranek, H. Lischka, and A. Karpen, *Journal of Chemical Physics* **91**, 5154 (1989).
- 33 W. Rijks and P. E. S. Wormer, *Journal of Chemical Physics* **90**, 6507 (1989).
- 34 P. R. Bunker, P. Jensen, A. Karpfen, M. Kofranek, and H. Lischka, *Journal of Chemical Physics* **92**, 7432 (1990).
- 35 P. Jensen, P. R. Bunker, A. Karpfen, M. Kofranek, and H. Lischka, *Journal of Chemical Physics* **93**, 6266 (1990).
- 36 S. A. C. McDowell and A. D. Buckingham, *Chemical Physics Letters* **182**, 551 (1991).
- 37 S. Rybak, B. Jerzierski, and K. Szalewicz, *Journal of Chemical Physics* **95**, 6576 (1991).
- 38 M. Quack and M. A. Suhm, *Chemical Physics Letters* **183**, 187 (1991).
- 39 M. Quack and M. A. Suhm, *Journal of Chemical Physics* **95**, 28 (1991).
- 40 M. Quack and M. A. Suhm, *Chemical Physics Letters* **234**, 71 (1995).
- 41 S. C. Racine and E. R. Davidson, *Journal of Physical Chemistry* **97**, 6367 (1993).
- 42 S. K. Loushin, S. Liu, and C. E. Dykstra, *Journal of Chemical Physics* **84**, 2720 (1986).
- 43 M. D. Marshall, P. Jensen, and P. R. Bunker, *Chemical Physics Letters* **176**, 255 (1991).
- 44 D. H. Zhang and J. Z. H. Zhang, *Journal of Chemical Physics* **99**, 6624 (1993).
- 45 D. H. Zhang and J. Z. H. Zhang, *Journal of Chemical Physics* **98**, 5978 (1993).
- 46 D. H. Zhang, Q. Wu, J. Z. H. Zhang, M. von Dirke, and Z. Bacic, *Journal*

- of Chemical Physics* **102**, 2315 (1995).
- 47 Q. Wu, D. H. Zhang, and J. Z. H. Zhang, *Journal of Chemical Physics* **103**, 2548 (1995).
- 48 W. C. Necochea and D. G. Truhlar, *Chemical Physics Letters* **224**, 297 (1994).
- 49 W. C. Necochea and D. G. Truhlar, *Chemical Physics Letters* **231**, 125 (1994).
- 50 W. C. Necochea and D. G. Truhlar, *Chemical Physics Letters* **248**, 182 (1996).
- 51 J. G. Anderson, *Annual Review of Physical Chemistry* **38**, 489 (1987).
- 52 C. R. Pollack, F. R. Petersen, D. A. Jennings, J. S. Wells, and A. G. Maki, *Journal of Molecular Spectroscopy* **99**, 357 (1983).
- 53 C. Amiot and G. Guelachvili, *Journal of Molecular Spectroscopy* **51**, 475 (1974).
- 54 H. C. Longuet-Higgins, *Molecular Physics* **6**, 445 (1963).
- 55 P. R. Bunker, *Molecular Symmetry and Spectroscopy* (Academic Press, New York, 1979).
- 56 M. Quack, *Molecular Physics* **34**, 477 (1977).
- 57 I. M. Mills, *Journal of Chemical Physics* **88**, 532 (1984).
- 58 J. T. Hougen and N. Ohashi, *Journal of Molecular Spectroscopy* **109**, 134 (1985).
- 59 S. C. Althorpe, D. C. Clary, and P. R. Bunker, *Chemical Physics Letters* **187**, 345 (1991).
- 60 E. L. Silbert III, *Journal of Chemical Physics* **93**, 5022 (1989).
- 61 G. T. Fraser, *Journal of Chemical Physics* **90**, 2097 (1989).
- 62 P. R. Bunker, P. Jensen, and A. Karpfen, *Journal of Molecular Spectroscopy* **149**, 512 (1991).

- 63 H.-C. Chang and W. Klemperer, *Journal of Chemical Physics* **104**, 7830 (1996).
- 64 G. C. Hancock and D. G. Truhlar, *Journal of Chemical Physics* **90**, 3498 (1989).
- 65 S. Davis, D. T. Anderson, and D. J. Nesbitt, *Journal of Chemical Physics* **105**, 6645 (1996).
- 66 D. H. Zhang, Q. Wu, and J. Z. H. Zhang, *Journal of Chemical Physics* **102**, 124 (1995).
- 67 S. Davis, J. T. Farrell, D. T. Anderson, and D. J. Nesbitt, *Chemical Physics Letters* **256**, 157 (1995).
- 68 D. H. Zhang and J. Z. H. Zhang, *Journal of Chemical Physics* **98**, 5978 (1993).
- 69 M. von Dirke, Z. Bacic, D. H. Zhang, and J. Z. H. Zhang, *Journal of Chemical Physics* **102**, 4382 (1995).
- 70 K. A. Peterson and T. H. Dunning, *Journal of Chemical Physics* **102**, 2032 (1995).
- 71 C. L. Collins, K. Morihashi, Y. Yamaguchi, and H. F. Schaefer III, *Journal of Chemical Physics* **102**, 6051 (1995).
- 72 D. C. Dayton, K. W. Jucks, and R. E. Miller, *Journal of Chemical Physics* **90**, 2631 (1989).
- 73 R. E. Miller, *Accounts of Chemical Research* **23**, 10 (1990).
- 74 R. B. Le Blanc, J. B. White, and P. F. Bernath, *Journal of Molecular Spectroscopy* **164**, 574 (1994).
- 75 R. S. Ram, Z. Morbi, B. Guo, K.-Q. Zhang, P. F. Bernath, J. Vander Auwera, J. W. C. Johns, and S. P. Davis, *Astrophysical Journal Supplement Series* **103**, 247 (1996).
- 76 M. Quack and M. A. Suhm, *Theor. Chim. Acta* **93**, 61 (1996).
- 77 M. A. Suhm, *private communication* .
- 78 S. F. Boys and F. Bernardi, *Molecular Physics* **19**, 553 (1970).